REFERENCE: SAF/AC/RMI&DWD&AUTH/VR/001
ISSUE: 2/2022
DATE: 28/02/2022
PAGES: 68

AC SAF VALIDATION REPORT

Validated products:

IASI-MetopA, IASI-MetopB and IASI-MetopC

Total Ozone and ozone profiles

Identifier	Name	Acronym
O3M-44	IASI B Near Real Time O_3	MBI-N-O3
O3M-49	IASI B Near Real Time O_3 profile	MBI-N-O3PR
O3M-306	IASI C Near Real Time O_3	MCI-N-O3
O3M-315	IASI C Near Real Time O_3 profile	MCI-N-O3PR

Authors:

Name	Institute
Andy Delcloo	Royal Meteorological Institute of Belgium (RMI)
Katerina Garane	Laboratory of Atmospheric Physics/Aristotle University of Thessaloniki (LAP/AUTH)
Peggy Achtert	Deutscher Wetterdienst (DWD)

Reporting period: **December 2019 – November 2020**

Validation methods: Lidars and microwave radiometers (altitude range 15 – 60 km)
Balloon soundings (altitude range 0 – 30 km)
Dobson and Brewer observations (total column DU)

Input data versions: FORLI 201501

Data processor versions: v6.5 (1/10 pixels)

Table of Contents

Introduction to EUMETSAT Satellite Application Facility on Atmospheric Composition monitoring (AC SAF)

Background

The monitoring of atmospheric chemistry is essential due to several human-caused changes in the atmosphere, like global warming, loss of stratospheric ozone, increasing UV radiation, and pollution. Furthermore, the monitoring is used to react to threats caused by natural hazards as well as to follow up the effects of international protocols.

Therefore, monitoring the chemical composition of the atmosphere and its effect on the Earth's radiative balance is a very important duty for EUMETSAT. The target is to provide information for policy makers, scientists and the general public.

Objectives

The main objectives of the AC SAF is to process, archive, validate and disseminate atmospheric composition products (O_3, NO_2, SO_2, BrO, HCHO, H_2O, OClO, CO, NH3), aerosol products and surface ultraviolet radiation products. The majority of the AC SAF products are based on data from the GOME-2 and IASI instruments onboard *EUMETSAT's* Metop satellites.

Another important task besides the near real-time (NRT) and offline data dissemination is the provision of long-term, high-quality atmospheric composition products resulting from reprocessing activities.

Product categories, timeliness and dissemination

NRT products are available in less than three hours after measurement. These products are disseminated via EUMETCast, WMO GTS or the internet.

- Near real-time trace gas column (total and tropospheric O_3 and NO_2, total SO_2, total HCHO, CO) and high-resolution ozone profile
- Near real-time absorbing aerosol index (AAI) from main science channels and polarization measurement detectors
- Near real-time UV index, clear-sky and cloud-corrected

Offline products are available within two weeks after measurement and disseminated via dedicated web services at EUMETSAT and AC SAF.

- Offline trace gas column (total and tropospheric O_3 and NO_2, total SO_2, total BrO, total HCHO, total H_2O) and high-resolution ozone profile
- Offline absorbing aerosol index from main science channels and polarization measurement detectors

- Offline surface UV, daily doses and daily maximum values with several weighting functions

Data records are available after reprocessing activities from the EUMETSAT Data Centre and/or the AC SAF archives.

- Data records generated in reprocessing
- Lambertian-equivalent reflectivity
- Total OClO

Users can access the AC SAF offline products and data records free of charge by registering at the AC SAF web site.

More information about the AC SAF project, products and services: https://acsaf.org/

AC SAF Helpdesk: helpdesk@acsaf.org

Twitter: https://twitter.com/Atmospheric_SAF

Applicable AC SAF Documents

[ATBD] FORLI Algorithm Theoretical Basis Document SAF/O3M/ULB/FORLI_ATBD Issue 1, 20/02/2014

[PUM] Product User Manual, SAF/AC/ULB/PUM/003, Issue 1.1, 10/02/2022

Both documents are available at http://acsaf.fmi.fi in the *Documents* section.

Acronyms and abbreviations

ATBD	Algorithm Theoretical Basis Document
AUTH	Aristotle University of Thessaloniki
DOAS	Differential Optical Absorption Spectroscopy
DWD	Deutscher Wetterdienst
GDP	GOME Data Processor
GOME	Global Ozone Monitoring Experiment
LAP/AUTH	Laboratory of Atmospheric Physics/Aristotle University of Thessaloniki
Metop	Meteorological Operational satellite
MWR	Microwave Radiometers
NDACC	Network for the Detection of Atmospheric Composition Change
NH	Northern Hemisphere
RMI	Royal Meteorological Institute of Belgium
SH	Southern Hemisphere
SZA	Solar Zenith Angle
TOC	Total Ozone Column
WMO	World Meteorological Organization
WOUDC	World Ozone and UV Data Center

1. General Introduction

Since this is the first report on IASI ozone profiles, it contains the validation results of the IASI instruments onboard all three sensors (Metop A, Metop B and Metop C). It covers the time period December 2019 to November 2020. The horizontal resolution is 12 km².

Since this work was carried out in three different institutes, this document is split up into three separate parts. The first part contains the validation of the retrieved IASI ozone profiles using ozonesondes (chapter 2). This part validates the retrieved ozone profiles in the troposphere and the lower stratosphere. The second part (chapter 3) uses measurements with lidars and microwave radiometers to assess the performance IASI ozone profiles; primarily in the stratosphere from 20 to 60 km altitude (chapter 3). The third part of this report (chapter 4), covers the validation of the integrated ozone profile product through an intercomparison with ground truth data from spectrophotometers (Dobson and Brewer). Additionally, the consistency of the integrated ozone profiles of IASI-A, IASI-B and IASI-C is examined by intercomparison to the respective operational products from GOME-2A, GOME-2B and GOME-2C with the GDP 4.8 algorithm for total ozone (DLR product) (chapter 4). The outcome of the different validation parts is summarized in the summary and conclusions section at the end of this report.

Table 1.1 and 1.2 present the different accuracies which are considered to assess the quality of the ozone profile and total ozone products.

Table 1.1: Different intended accuracies for ozone profiles, provided in the Product Requirements Document SAF/AC/FMI/RQ/PRD/001

	Accuracy	
Threshold	**Target**	**Optimal**
30 % in stratosphere	15 % in stratosphere	5 % in stratosphere
50 % in troposphere	30 % in troposphere	10% in troposphere

Table 1.2: As in Table 1.1 for total ozone accuracies.

	Accuracy	
Threshold	**Target**	**Optimal**
20 %	4 % (SZA < 80°) 6 % (SZA > 80°)	1.5 %
Verification method	Comparison with ground-based measurements	

2. Validation of ozone profiles using ozonesondes

2.1 Introduction

This chapter presents validation results for the AC SAF IASI ozone profile product. The validation was carried out using ozone sounding profiles.

Ozonesondes are lightweight balloon-borne instruments which measure ozone concentrations from the surface up to about 30 km with much better vertical resolution than possible from satellite data. In general, measurement precision and accuracy are also better compared to satellite observations, at least in the lower stratosphere and the troposphere. Another advantage is that ozone soundings can be performed at any time and during any meteorological condition.

The precision of ozonesondes varies with altitude and depends on the type of ozonesonde used. Table 2.1 shows indicative precision of the Electrochemical Concentration Cell (ECC) at different pressure levels of the sounding.

Table 2.1: Precision (in percent) of different types of ozonesondes at different pressure levels.

Pressure level (hPa)	ECC
10	2
40	2
100	4
400	6
900	7

Profiles from ozonesondes are most reliable around the 40 hPa level, which is around the ozone maximum. The error bar of profiles from ozonesondes increases rapidly at levels above the 10 hPa level, which is at around 31 km altitude.

2.2 Dataset description

IASI ozone data used in this validation report covers the time period from December 2019 to November 2020. IASI ozone profile data are used for pre-selected sites where ozone soundings are performed on a regular basis. Ozonesonde data was made available by the World Ozone and Ultraviolet Data Center (WOUDC). (http://www.woudc.org) and the NILU's Atmospheric Database for Interactive Retrieval (NADIR) at Norsk Institutt for Luftforskning (NILU) (http://www.nilu.no/nadir/). In Table A.3, an overview is shown from the ozonesonde station data used in this report. The location of the stations is summarized in Figure 2.1, the collocation data in Figure 2.2.

Figure 2.1: Stations consulted for validation.

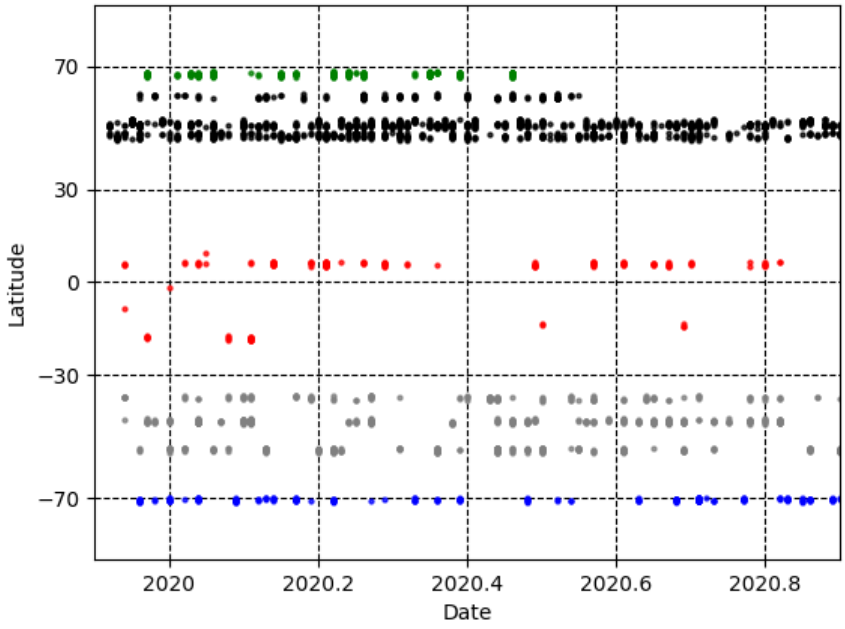

Figure 2.2: Spatial and temporal representation of the collocation data used for the validation with ozonesonde data for the period December 2019 – November 2020 for IASI-B.

Ozonesonde data are generally made available by the organization carrying out observations after a short delay related to data quality assurance. Nevertheless, some organizations make their ozone profile data readily available for validation purposes.

Table A.3 of the Appendix shows an overview of the station data used in this validation report using ozonesondes and the collocations in space and time are shown in Figure 2.2 for IASI-B.

2.3 Comparison procedure

2.3.1 Co-location criteria

The selection criteria are twofold:

- The geographic distance between the IASI pixel center and the sounding station location is less than 100 km.
- The time difference between the pixel sensing time and the sounding launch time is less than ten hours.

Each sounding that is correlated with a IASI overpass is generally correlated with several IASI pixels if the orbit falls within this 100 km circle around the sounding station. This means that a single ozone profile is compared to more than one IASI measurement.

2.4 Ozone sounding pre-processing

IASI ozone profiles are given as partial ozone columns on 40 fixed 1 km altitude levels. Ozone partial columns are expressed in Dobson Units.

Ozonesondes measure ozone concentration along the ascent with a typical vertical resolution of 100 m while IASI profiles consist 40 layers between the ground and 40 km asl. The last layer available is from 40 km to 60 km asl. Ozonesondes give ozone concentration in partial pressure. The integration requires interpolation, as IASI levels never match exactly ozonesonde layers. This interpolation causes negligible errors given the high vertical resolution of ozonesonde profiles.

For comparison, ozonesonde profiles are integrated between the IASI pressure levels. When a single ozonesonde profile is compared to different IASI profiles, the actual reference ozone values are not the same given that the IASI level boundaries vary from one measurement to another. Integrated ozonesondes data will be referred to in this report as X_{sonde}.

IASI layers are relatively thick and IASI layer boundaries show small variations compared to the layer thickness. Hence, individual layers generally occur around the same altitude. The altitude of those layers can be considered as "fixed" and therefore the center of an "*averaged layer altitude (or pressure)*" is used in plotting the data.

In this report, the validation of the IASI profiles is calculated by using the averaging kernels (AVK) of the IASI profile. The motivation to apply the AVK is to "smooth" the ozone soundings towards the resolution of the satellite:

$$X_{avk\_sonde} = X_{apriori} + A\,(X_{raw\ sonde} - X_{apriori}) \qquad (1)$$

Where A represents the averaging kernel, X_{avk_sonde} is the retrieved ozone sonde profile, X_{sonde} is the ozone sonde profile and $X_{apriori}$ is the a priori profile.

2.5 Results

2.5.1 Difference profiles

The relative difference between the ozone profiles from IASI and an ozonesonde is calculated as:

$$(X_{IASI} - X_{sonde})/X_{sonde.} \quad (2)$$

For comparing the IASI ozone profile with the smoothed ozonesonde profiles (AVK ozonesondes) the following equation is used:

$$(X_{IASI} - X_{AVK\text{-}SONDE})/X_{AVK\text{-}SONDE} \quad (3)$$

Figure 2.3 shows relative difference profiles between IASI ozone profiles at the one hand and on the other hand ozonesonde-, and AVK ozonesonde profiles for different latitude belts for IASI-A, IASI-B and IASI-C for one year of data.

In the next sections, we will discuss the seasonal behavior and other possible influences on the quality of the ozone profile product.

For the polar and midlatitude stations, the difference plots in Figure 2.3 show that IASI ozone profiles are within the optimal error range of 10%, compared to the ozonesonde reference, except for the Upper Troposphere – Low Stratosphere (UTLS) region. For the troposphere, most of the latitude belts show relative differences within 30%. Applying the averaging kernels, improves the comparison significantly.

Since the tropospheric integrated ozone column product is not an official operational product, we will also discuss the results on the tropospheric ozone profile.

Table 2.1 provides an overview of the height ranges related to the troposphere, the UTLS-zone and the lower stratosphere. Considering these definitions, we are calculating the statistics for the troposphere and the lower stratosphere. The higher stratosphere statistics are shown in Chapter 3.

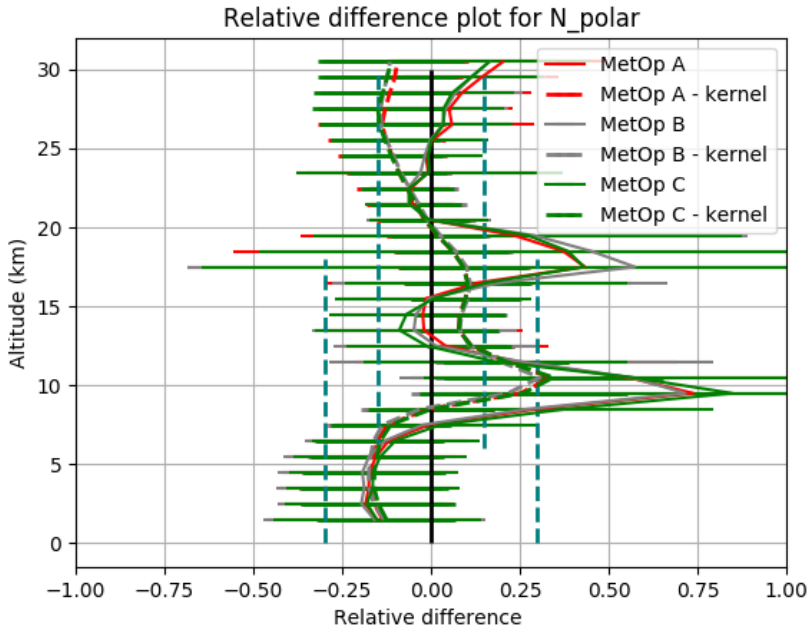
Relative difference plot for N_polar
MetOp A
MetOp A - kernel
MetOp B
MetOp B - kernel
MetOp C
MetOp C - kernel
Altitude (km)
Relative difference

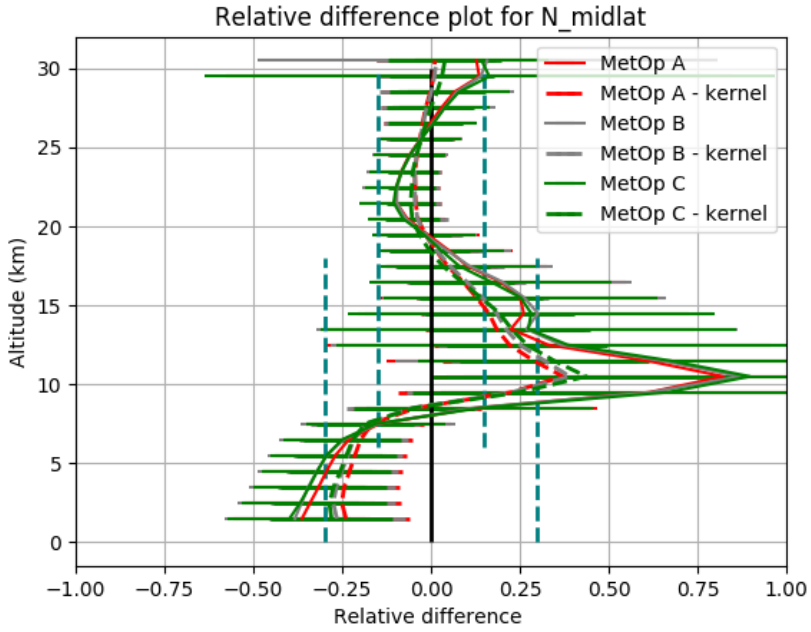
Relative difference plot for N_midlat
MetOp A
MetOp A - kernel
MetOp B
MetOp B - kernel
MetOp C
MetOp C - kernel
Altitude (km)
Relative difference

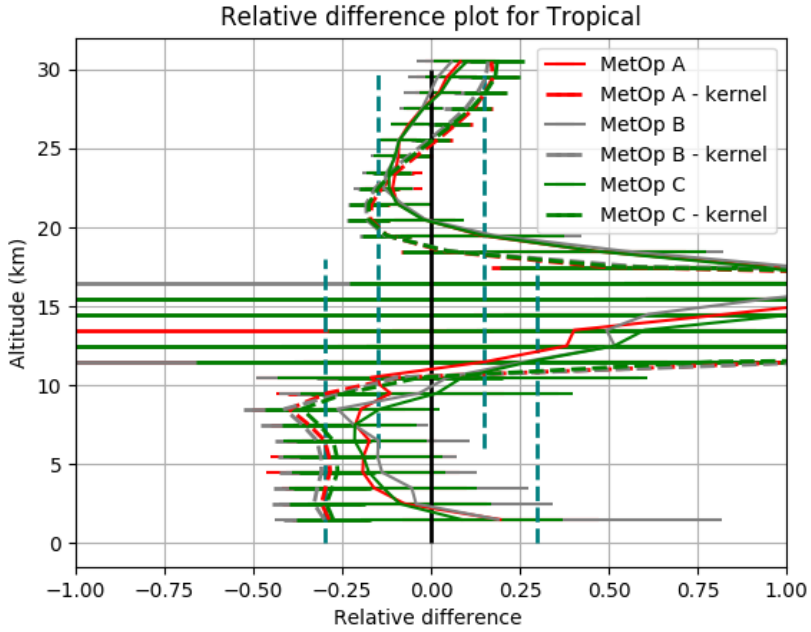
Relative difference plot for Tropical
MetOp A
MetOp A - kernel
MetOp B
MetOp B - kernel
MetOp C
MetOp C - kernel
Altitude (km)
Relative difference

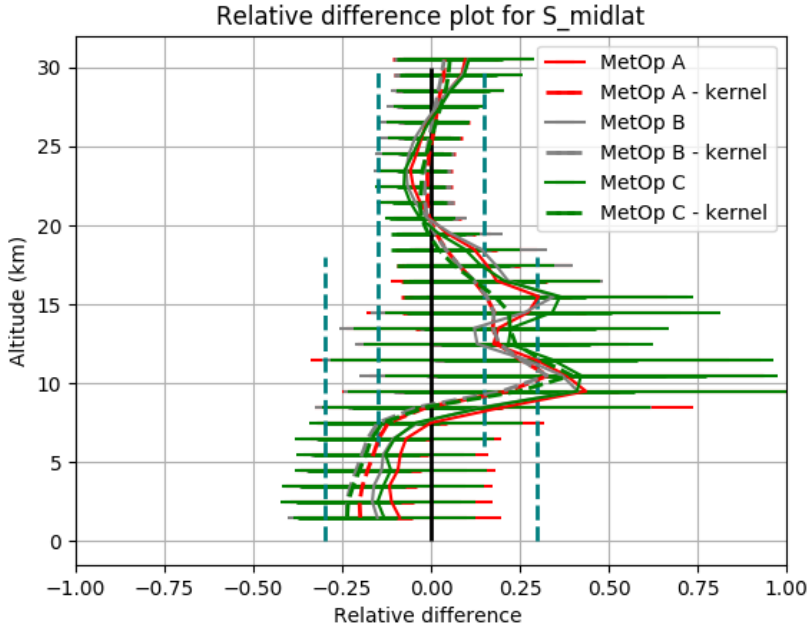
Relative difference plot for S_midlat
MetOp A
MetOp A - kernel
MetOp B
MetOp B - kernel
MetOp C
MetOp C - kernel
Altitude (km)
Relative difference

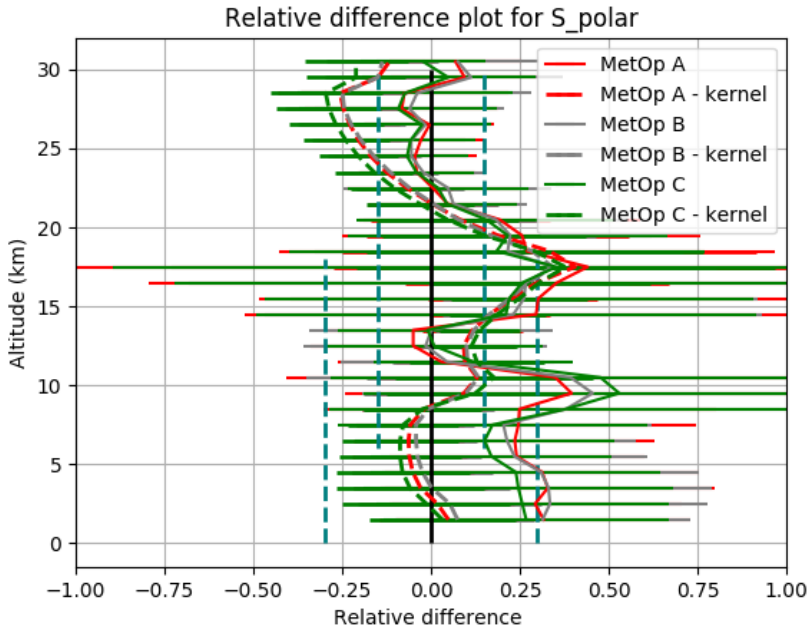

Figure 2.3: Relative difference in ozone profiles from IASI, ozonesondes and smoothed ozonesondes according to equations (2) and (3) for different latitude belts and for different sensors (IASI-A/B/C) for the period December 2019 to November 2020. The error bars represent one standard deviation on the mean error. The green dashed lines are the target values for stratospheric (15 %) and tropospheric (30 %) ozone according to Table 1.1.

Table 2.1: Definition of the ranges in km for troposphere, UTLS-zone and stratosphere for the different latitude belts.

	Troposphere	UTLS	Lower Stratosphere
Polar Regions	< 6 km	6 km - 12 km	12 km - 30 km
Mid-Latitudes	< 8 km	8 km - 14 km	14 km - 30 km
Tropical Regions	< 12 km	12 km - 18 km	18 km - 30 km

Table 2.2: Relative Differences (RD) and standard deviation (STDEV) of IASI ozone profiles product with respect to XAVK-sonde for the troposphere, considering five latitude belts for the period December 2019 – November 2020.

	troposphere IASI-A			troposphere IASI-B			troposphere IASI-C		
	AD (DU)	RD (%)	STDEV (%)	AD (DU)	RD (%)	STDEV (%)	AD (DU)	RD (%)	STDEV (%)
northern polar region	-2.69	-15.92	19.22	-2.78	-16.20	19.18	-2.49	-14.88	20.06
northern midlatitudes	-4.62	-22.01	15.57	-5.04	-24.19	16.46	-5.21	-24.83	14.80
tropical regions	-5.93	-16.64	33.40	-6.21	-17.12	32.55	-5.47	-16.32	24.00
southern midlatitudes	-3.06	-17.14	15.29	-3.59	-20.43	14.34	-3.48	-19.64	14.86
southern polar region	-0.37	-1.48	18.58	-0.10	1.36	21.44	-0.73	-4.14	20.18

Table 2.3: Relative Differences (RD) and standard deviation (STDEV) of IASI ozone profiles product with respect to XAVK-sonde for the lower stratosphere, considering five latitude belts for the period December 2019 – November 2020.

	Lower stratosphere IASI-A			Lower stratosphere IASI-B			Lower stratosphere IASI-C		
	AD (DU)	RD (%)	STDEV (%)	AD (DU)	RD (%)	STDEV (%)	AD (DU)	RD (%)	STDEV (%)
northern polar region	-4.3	-1.6	15.5	-3.8	-1.5	15.0	-4.7	-2.0	15.0
northern midlatitudes	-1.5	1.0	11.6	-1.0	1.3	12.4	-2.1	1.0	11.4
tropical regions	-1.3	-1.5	5.9	-4.0	-3.0	6.3	-2.4	-1.9	6.3
southern midlatitudes	3.4	4.0	12.8	2.6	3.5	12.2	1.9	3.8	12.8
southern polar region	-5.8	2.6	23.3	-4.4	2.0	20.2	-7.0	0.3	20.1

*The relative difference statistics are derived as a weighted average over the lower- and upper stratospheric ozone profile levels. The absolute differences however are integrated over respectively the lower- and upper stratospheric ozone profile levels.

Table 2.3 shows an overview of the obtained results for all sensors for the troposphere. For the ozone profile product, the target values (25 %) are met. Table 2.3 shows the statistics for all the sensors for the lower stratosphere. For all the latitude bands, the optimal value is met (5 %). Both statistics for troposphere and lower stratosphere, confirm that there is a very high consistency between the different sensors, which makes it a very promising product for climate change monitoring.

2.5.2 Scatter plots for the retrieved ozone partial columns

Scatter plots for different altitude levels are plotted in Figure 2.4, showing the retrieved ozone partial columns as a function of the reference partial column measured by ozonesondes. This is shown in Figure 2.4 for the northern midlatitude stations at six different altitude levels. In order to evaluate these ozone profile layers as seen by the satellite, we will smooth the ozone profile layers by applying the averaging kernels. This is shown in Figure 2.5. We observe that the slope values indeed improve significantly (closer to 1) while the intercept values are closer to 0.

The interpretation of "better results" should be taken with care. Applying the kernels using equation 1 is a way to smooth the ozone profile towards a comparable vertical resolution of the retrieved ozone profile. High resolution effects like filaments present for example in secondary ozone maxima are mostly not seen by IASI which results in sometimes large differences between observed and retrieved partial ozone columns. The regression line in the scatter plots show therefore that IASI loses sensitivity in the lower troposphere and around the UTLS-zone (Figure 2.4). We can conclude that upon smoothing matching, the agreement improves.

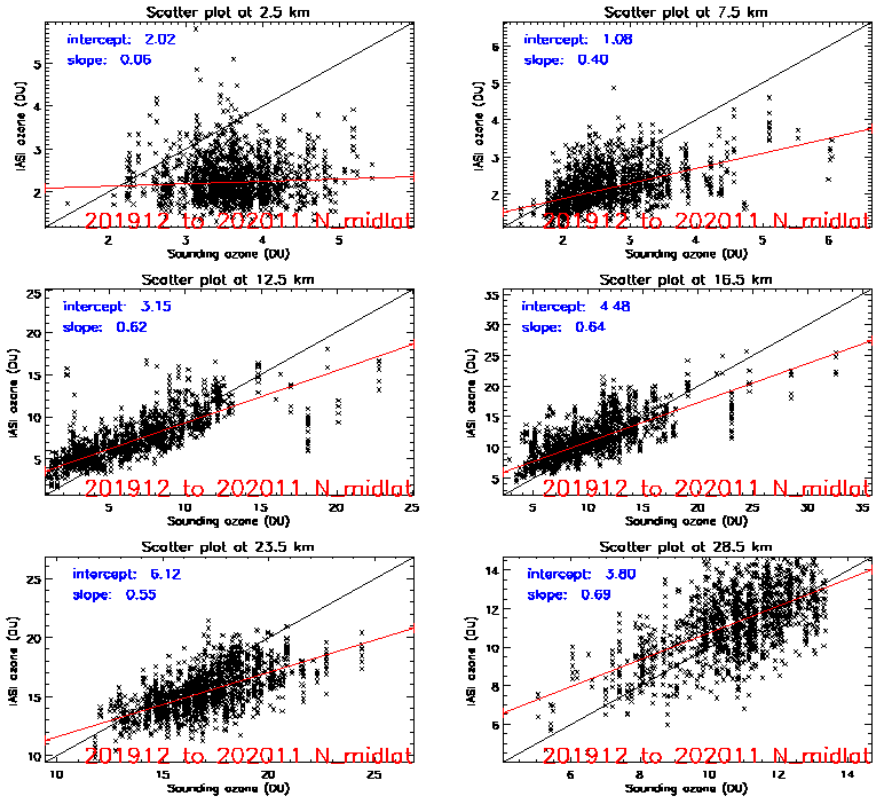

Figure 2.4: Scatter plot at 6 different altitude levels for the stations at northern midlatitudes (January 2013- December 2018, IASIB).

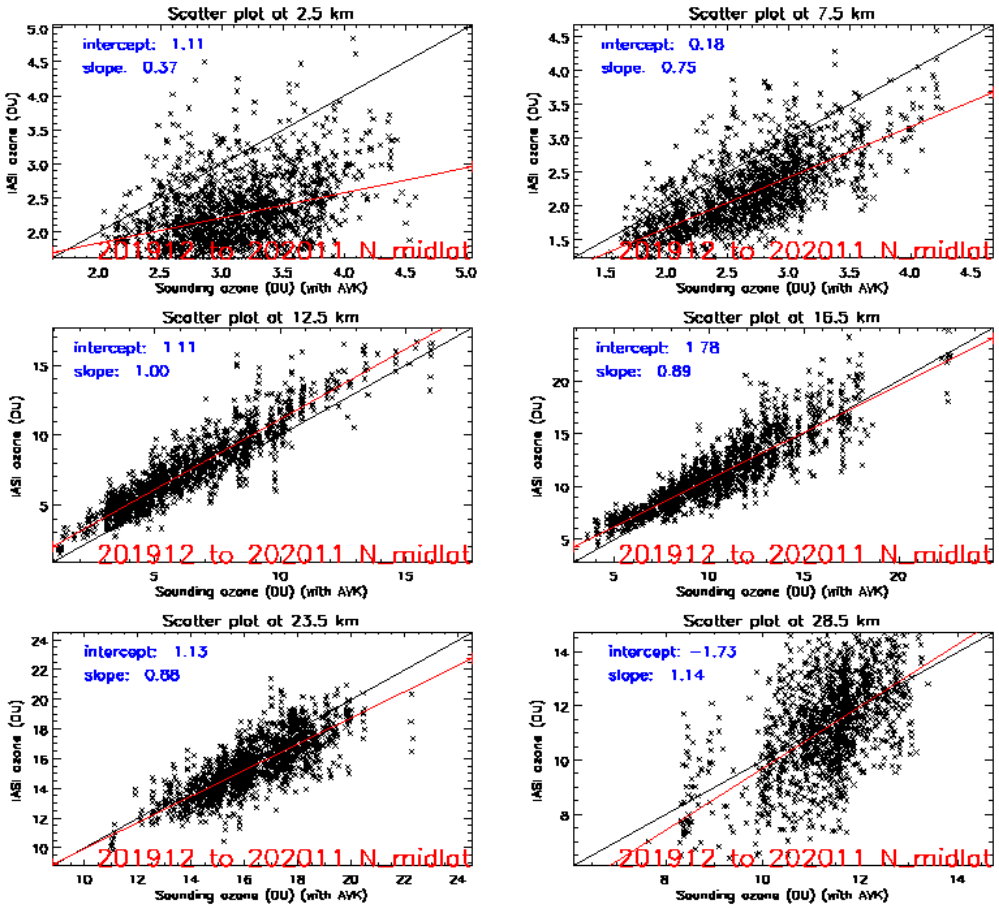

Figure 2.5: Scatter plot at 6 different altitude levels for the stations at northern midlatitudes (January 2013- December 2018, IASIB), applying the kernels

Examining some dependencies on the quality of the retrieved ozone profile shows that there is a seasonal dependency present in the time series. The Solar Zenith Angle (SZA), more specifically at higher latitudes (polar stations), hereby also influences the product. This is especially visible in the higher layer in the lower stratosphere, when comparing Figure 2.6 and Figure 2.7. Besides this influence on SZA, the dependence on cloud cover is not verified, since we only consider ozone profiles with a cloud cover lower than 13 %.

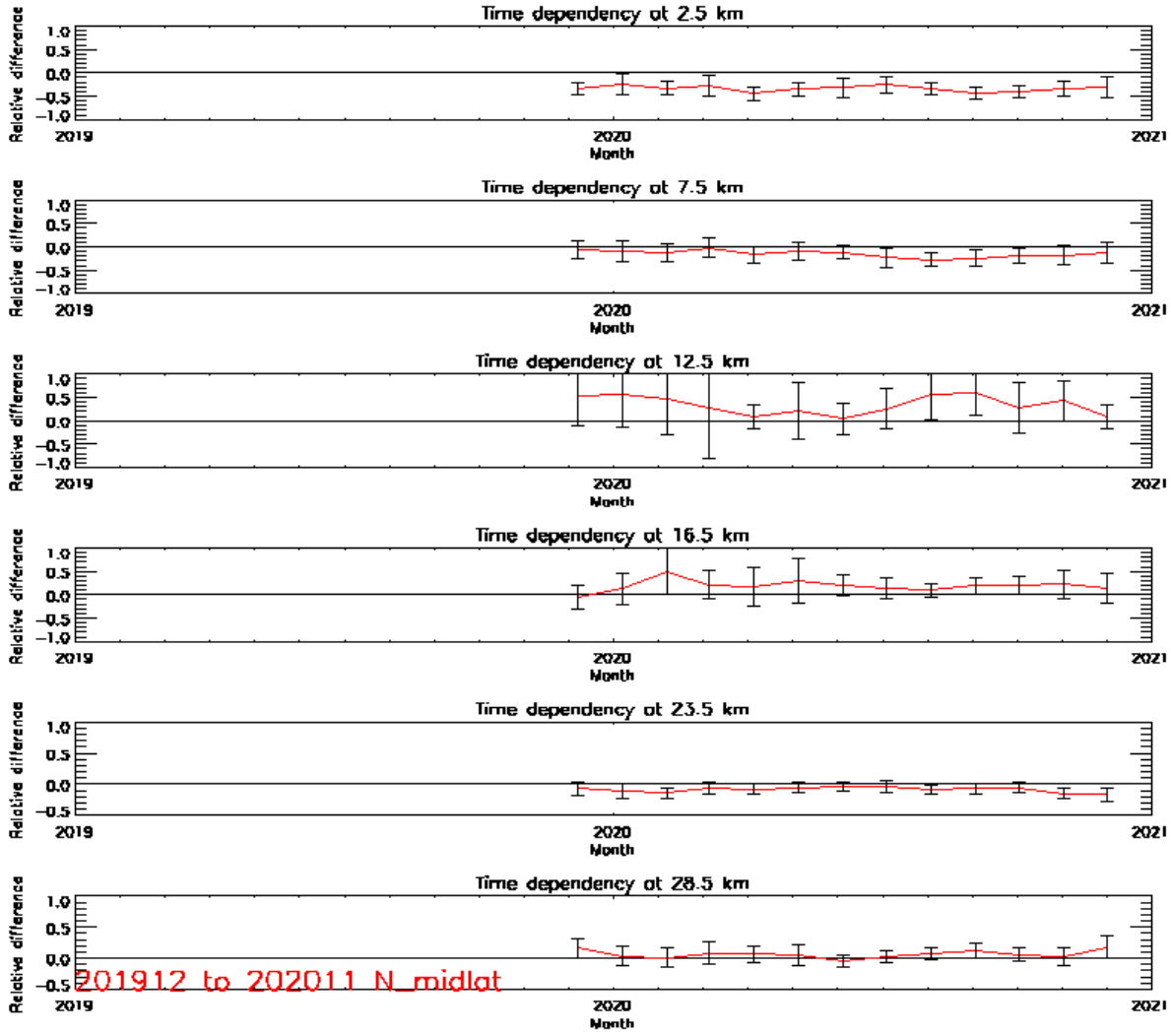

Figure 2.6: Time series at 6 different altitude levels for the stations at northern midlatitudes (December 2019 – November 2020) for the IASI-A time series.

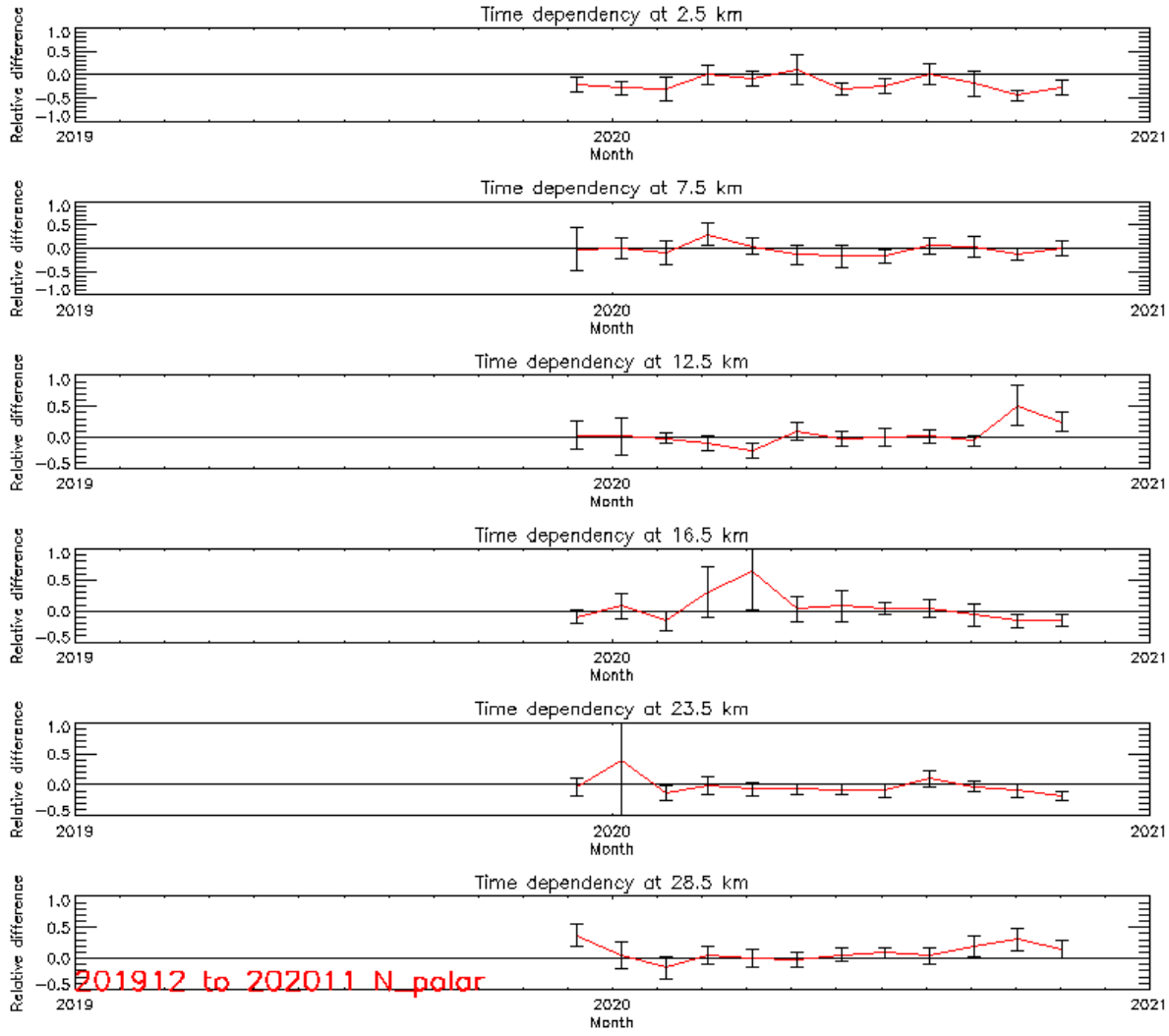

Figure 2.7: Time series at 6 different altitude levels for the northern polar stations (December 2019 – November 2020) for the IASI-A time series.

2.5.3 Median sensitivity

According to Keppens et al., 2015, it is interesting to have a more detailed look to the averaging kernels, which can be seen as the vertical sensitivity of the ozone profile product. The best way to do it in an intuitive way is to observe the evolution of the median sensitivity in function of time and vertical profile. Here we only look at the median sensitivity until an altitude of about 30 km for northern midlatitude station (Figure 2.8). We also observe here that there is a seasonal variation present for the whole profile. When we compare the median sensitivity plots for the northern polar stations (upper panels) against the median sensitivity plots for the northern mid-latitude stations (lower panels) for IASI-A (left panels) and IASI-B (right panels), it is shown

how for both latitudes there is a specific behavior present. Also the seasonal behavior, present in the product is visible here.

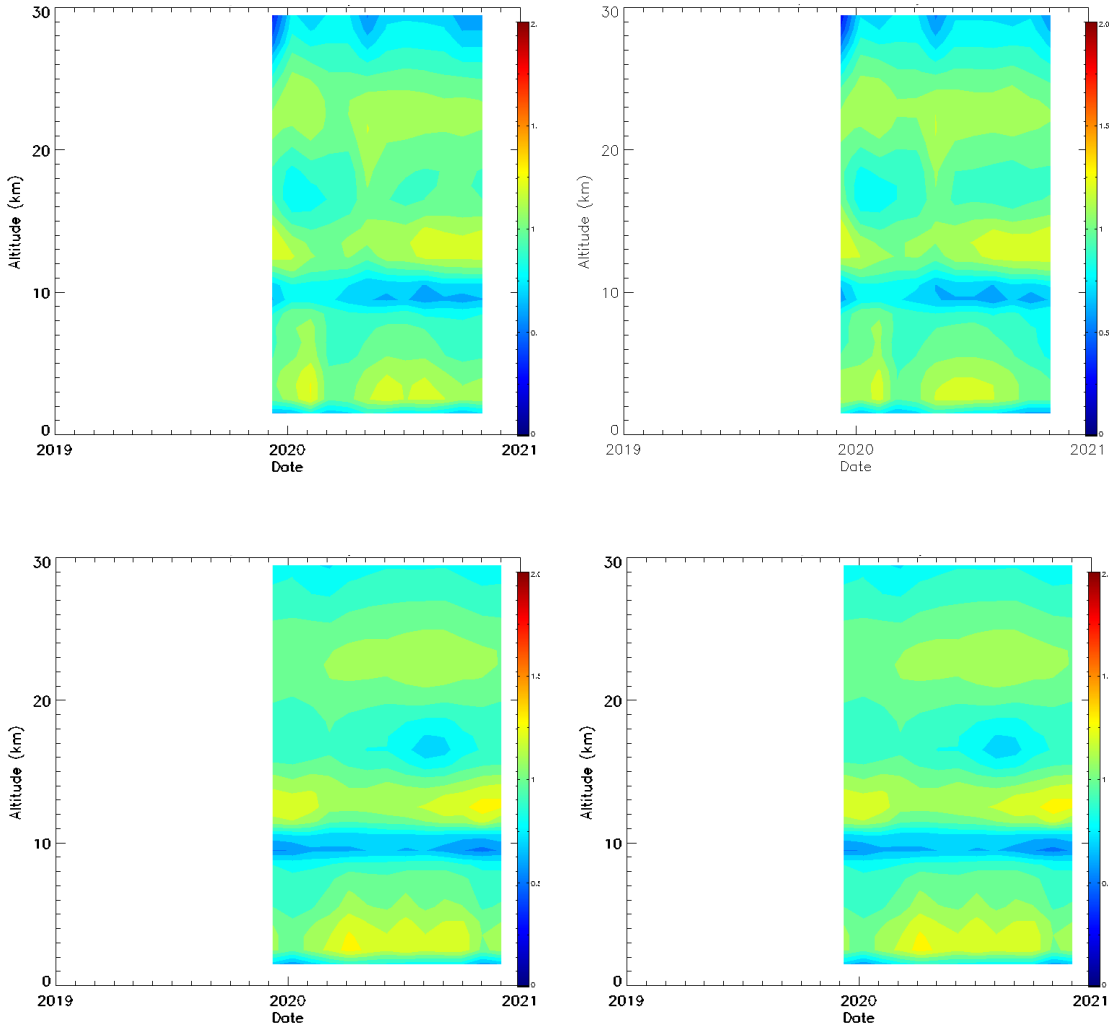

Figure 2.8: Median sensitivity plot (1 -30 km) from collocated data for IASIA (left) and IASIB (right) according to Keppens et al., 2015. Above are the median sensitivity plots, derived for the northern polar stations, below are the median sensitivity plots derived for the northern midlatitude stations.

2.6 General conclusions for the validation of ozone profiles, using ozonesondes

The IASI-A/B/C vertical ozone profile products are validated against ozonesonde data. The validation results have revealed the following properties:

- The comparisons of the ozone profile product with ozonesondes for all sensors show almost exactly the same results and are all within optimal value (5 %) for the lower stratosphere (Table 2.2) and target value (30 %) for the troposphere (Table 2.3).
- In general, we observe an underestimation in the troposphere and the lower stratosphere. The UTLS zone shows an overestimation.
- IASI ozone profile retrievals show a seasonal dependency, especially higher up in the profile and is also latitudinal dependent (more influenced towards the poles)
- The median sensitivity plots show a stable and comparable 'fingerprint' between both sensors.

3. Validation of ozone profiles with lidar and microwave instruments

3.1 Dataset description

In this validation report EUMETSAT data processed with FORLI 201501, processor v6.5 (1/10 pixels), for the time period from December 2019 to November 2020, are used. Absolute differences (AD), relative Differences (RD), and standard deviation (STDEV) of IASI A, B, and C ozone profile products versus ground-based reference profiles for the lower and upper stratosphere and different latitude belts were calculated for the time period under investigation. Only data with a quality flag equal to one were used, since the recommended quality flay equal to two for validation is currently not provided in the data set. Averaging kernels were determined following the method described in *EUMETSAT 2017.* The standard deviation and variance are determined using the error covariance matrix provided in the data set.

The main ground-based instruments available for validation purposes in the upper stratosphere are lidars and microwave radiometers (MWR). Their altitude range typically covers 15 km to 50 or 60 km. This significantly extends the range covered by ozonesondes towards higher altitudes, including a good overlap from 15 to 30 km altitude. Note that there are only about 10 operational lidar and MWR stations on the globe that provide regular data, though not as rapidly and operationally as the ozonesonde stations. The ground-based validation profiles come from NDACC (Network for the Detection of Atmospheric Composition Change, http://www.ndsc.ncep.noaa.gov/). NDACC lidar and microwave instruments go through an evaluation process and have to pass thorough quality checks (Keckhut et al., 2004). The ozone profiles are not available in near real time. A minimum of one month is necessary before profiles become available but most stations need three or more months. NDACC demands that ozone profiles are submitted at least once per year to their database. The stations (Figure 3.1) used in this validation for the lidar/microwave data are: Ny-Ålesund (microwave, 78.92° N, 11.93° E), Hohenpeissenberg (lidar, 47.8° N, 11.0° E), Bern (microwave, 46.95° N, 7.45° E), Haute-Provence (lidar, 43.94° N, 5.71° E), Table Mountain (lidar, 34.4° N, 117.7° W), Mauna Loa (lidar and microwave, 19.54° N, 155.58° W), and Lauder (lidar and microwave, 45.04° S, 169.68° E). Mean statistics are calculated for polar stations located between 65°N and 90° N, mid-latitude stations between 25° N and 65° N, and tropical stations located between 25° N and 25° S. The NDACC stations considered for the comparisons are also listed in Tables A.4 (Appendix 1).

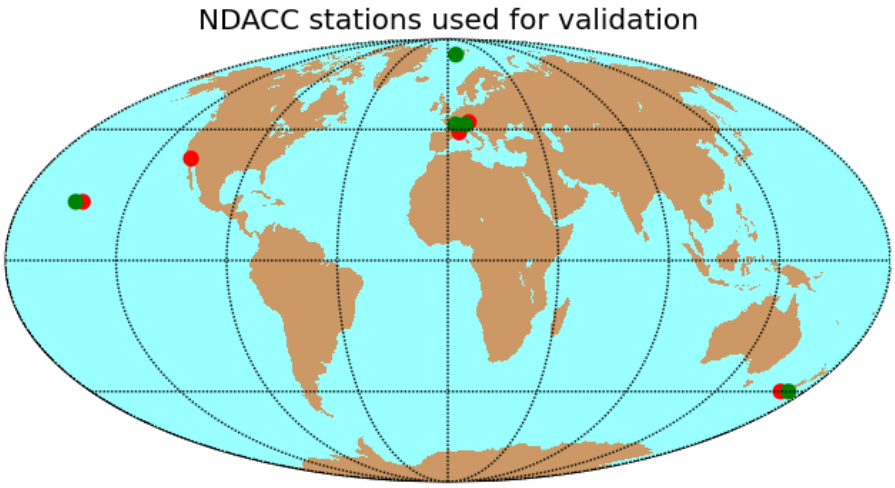

Figure 3.9: Stations consulted for validations. Lidar stations in red and microwave radiometer station in green.

3.2 Comparison procedure

Generally, the comparison procedure is the same as for the ozonesondes, outlined in Section 2 (see also Delcloo and Kins, 2009; 2012). Different temporal resolution and measurement frequency of the ground-based instruments, however, require some minor changes.

3.3 Co-location criteria in time and space

Only ground-based and satellite profiles that are close in space and in time to IASI profiles are compared. Nightly mean lidar measurements are compared to IASI profiles measured either in the morning after or the morning before the lidar profile. This means that a maximum time difference of 20 hours is allowed. Figure 4.13, shows the spatio-temporal distribution of the co-locations of the ground-based measurements to IASI Metop C as an example.

MWR measure around the clock, typically one profile every hour. So usually MWR profiles can be compared with IASI ozone profiles measured within less than 2 hours. Usually all IASI measurements are made during local morning.

Only IASI profiles with ground pixel centers closer than 200 km to a validation stations were considered. A 200km radius typically gives about 20 co-located IASI profiles per station and orbit. As a minimum 3 co-located IASI profiles per station and orbit are needed. Larger co-location radii result in larger geophysical differences, smaller radii result in too few comparisons cases.

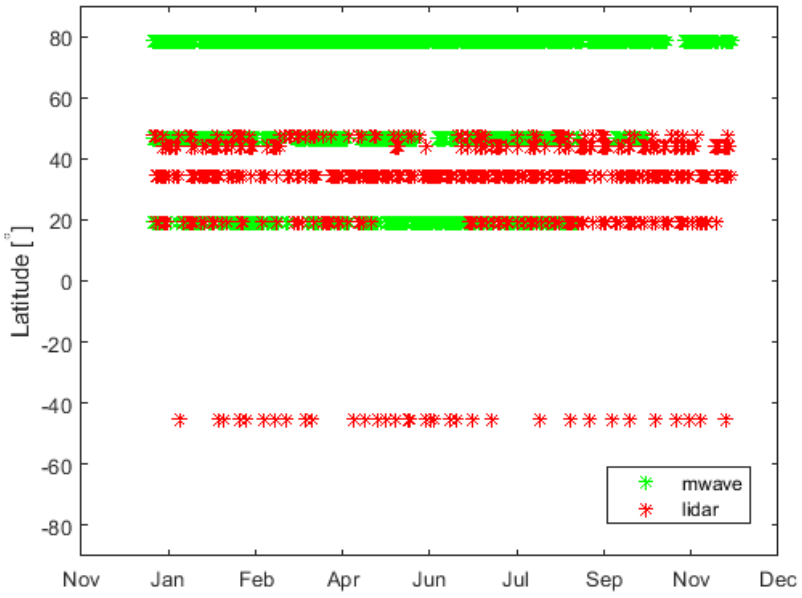

Figure 3.2: Spatial and temporal representation of the co-location data used for the validation with ground-based measurements (mwr: green, lidar: red) for the time period December 2019 to November 2020.

3.4 Pre-processing of the ground-based ozone profiles.

Like the ozonesonde data, lidar and MWR ozone number density profiles are first averaged over the IASI retrieval layers, usually 40 layers, about 1 km deep. The resulting slightly smoothed profiles are called Xref.

In the next step, the Xref lidar and MWR profiles are further smoothed over altitude by applying the IASI averaging kernels (with proper scaling). These smoothed profiles XAVK have an altitude resolution comparable to the IASI profiles (or coarser).

Since the IASI measurement alone does not fully constrain the retrieved ozone profile, IASI profiles are a mix of measured information and a-priori "climatological" ozone profiles. For the validation of the retrieval process, it makes sense to also consider reference profiles that have been smoothed by the averaging kernels, and have the same mix of measured and a-priori profile as the IASI profiles. The resulting profiles are called XAVK apriori in the following. An example, showing lidar profiles measured at Hohenpeissenberg station and the determined XAVK profiles, is provide in Figure 3.3 left panel. Note that the IASI averaging kernels vary slightly from profile to profile. This results in small differences in the smoothed lidar profiles. The absolute and relative difference between lidar and IASI-B ozone profile are shown in the middle and right panel.

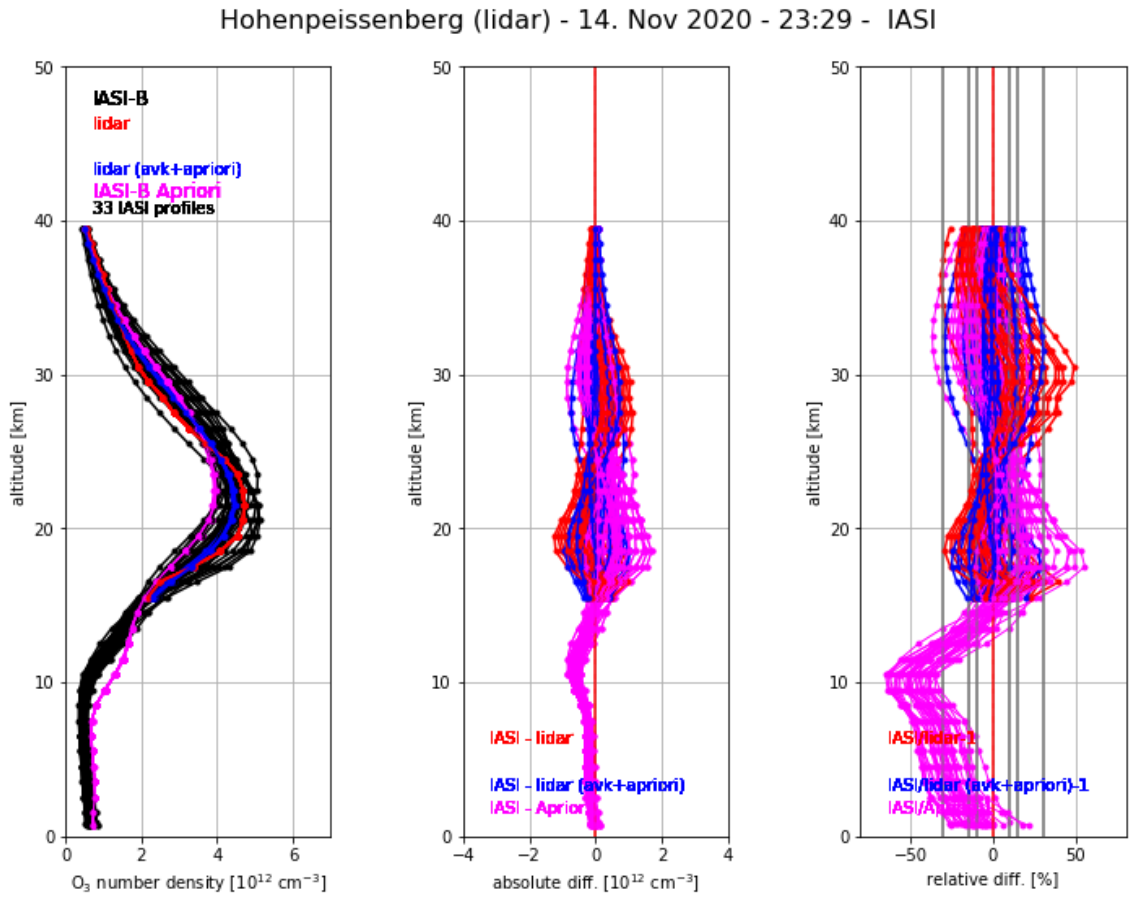

Figure 3.10: Example for the comparison of a lidar profile at Hohenpeissenberg, Germany, (red Xref, blue XAVK, apriori) with the matching IASI Metop-B profiles (black). Left panel: Absolute values. Middle panel: Absolute differences. Right panel: Relative differences.

3.5 Results

This summary contains validation results for the time periode between December 2019 and November 2020. To report the quality of IASI ozone profile products in a very condensed way, the statistics for the different output levels of IASI can be reduced to two layers: Lower Stratosphere (up to an altitude of 30 km) and Upper Stratosphere (above 30 km, up to 50 or 60 km). Table 3.1 shows the definition of the height ranges for lower and upper stratosphere for different latitude belts used in this report.

Table 3.1: Definition of the ranges for lower and higher stratosphere for the different latitude belts.

	Lower Stratosphere	Upper Stratosphere
Polar Region	12 km – 30 km	30 km – 50 km
Mid-Latitudes	14 km – 30 km	30 km – 50 km
Tropical Region	18 km – 30 km	30 km – 50 km

The validation for the lower stratosphere is made using ground-based ozonesonde data as a reference. For the upper stratosphere, ground-based lidar and microwave data are used as reference.

Relative differences (Eq. 1) are calculated against the ground-based reference data. Usually these are also convolved with the averaging kernels, including the a-priori contribution (Smoothed ground-based):

$$\frac{\text{(IASI – Smoothed ground-based profile)} * 100}{\text{Smoothed ground-based profile}} \qquad (1)$$

The collocation between IASI and the ground-based station is shown for one example station in Figure 3.4. For the validation only, IASI data within a radius of 200 km and with a time delay smaller than 2 hours for mwr and 4 hours for lidar are considered.

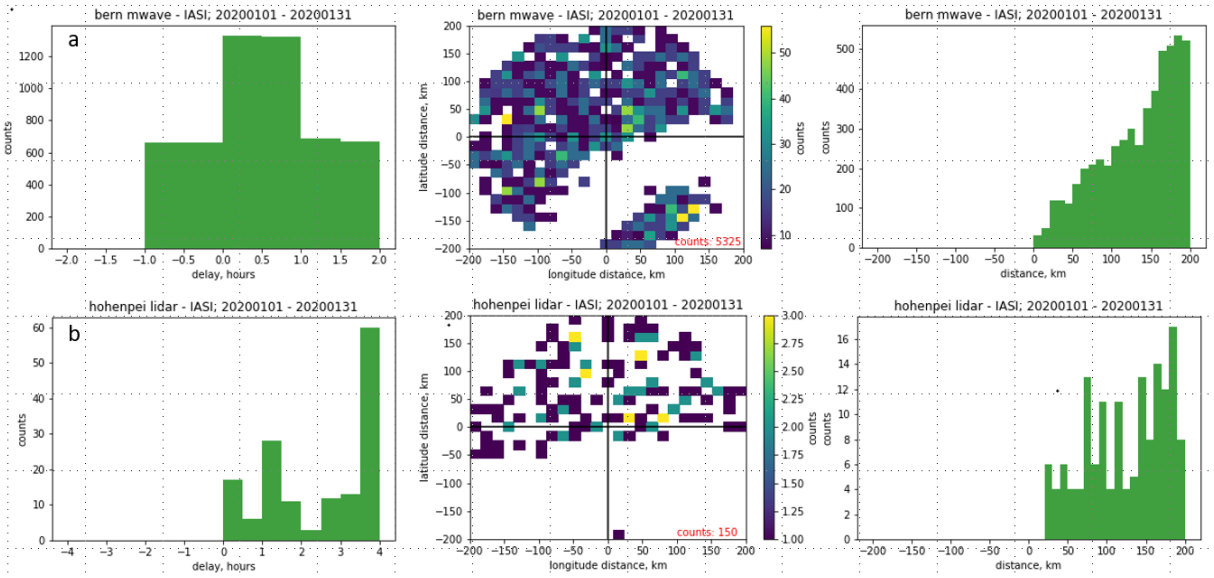

Figure 3.4: Examle for the collocation between the lidar station at Hohenpeissenberg (a), the mwr station in Bern (b) and IASI on Metop C. The left panel shows IASI counts versus delay to the ground-based observations, the middle panel shows latitude and longitude distance between IASI and the ground stations, and the right panel shows the IASI counts per distance.

The time series of the monthly mean difference between IASI and the reference station in Figure 3.5 demonstrate that IASI A, B, and C are in very good agreement and there is no difference between the different instruments. There is also no degradation or drift visible. However, in autumn at higher latitudes (Figure 3.5b), larger differences between IASI and the reference station are observed. As observed in the troposphere and lower stratosphere it could be a seasonal dependency, but there could also be an instrument problem with the microwave radiometer at Ny Alesund. A longer timeseries is needed to confirm a seasonal dependency for stratospheric profiles at high latitudes.

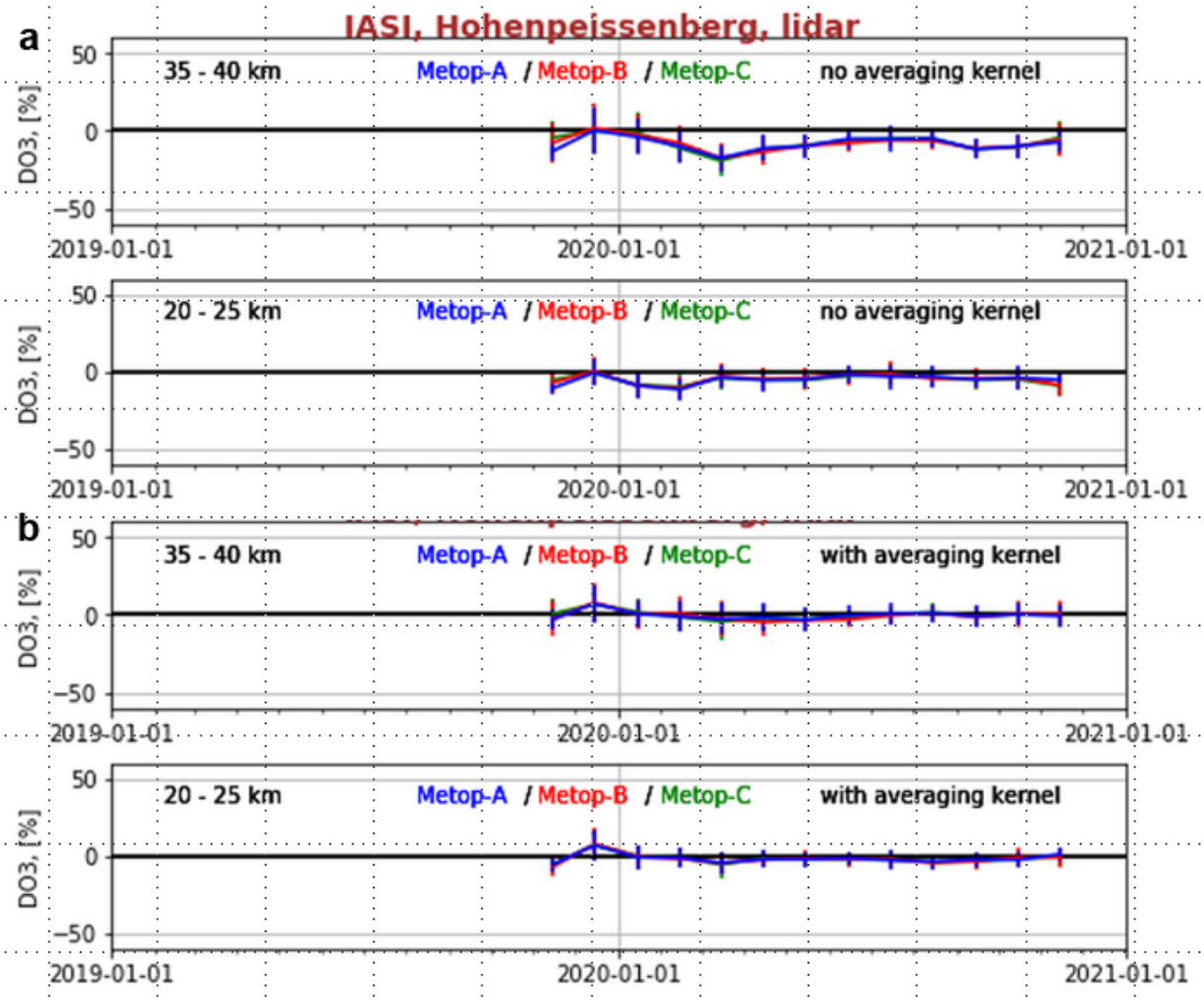

Figure 3.5a: Time series of monthly mean difference without averaging (a) and with averaging kernel (b) between IASI A (blue), B (red), and C (green) and ground-based NDACC lidar ozone measurements at Hohenpeissenberg.

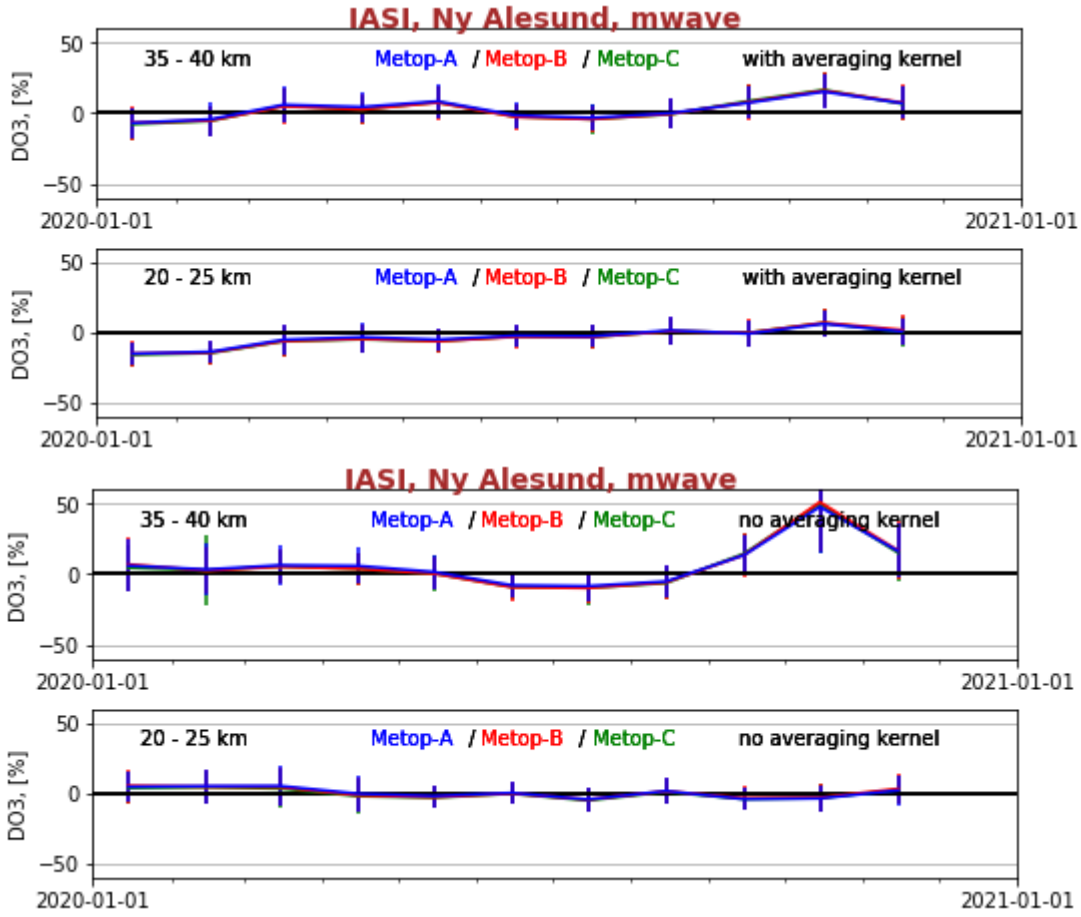

Figure 3.5b: Time series of monthly mean difference without averaging (a) and with averaging kernel (b) between IASI A (blue), B (red), and C (green) and ground-based NDACC mwave ozone measurements at Ny Alesund.

Table 3.2 summarizes the overall difference between IASI A, B and C ozone profiles and ground-based reference profiles for the time period from December 2019 to November 2020, for the lower and upper stratosphere. The relative difference statistics are derived as a weighted average over the lower- and upper stratospheric ozone profile levels. The absolute differences however the lower- and upper stratospheric ozone profile levels are integrated over respectively. Tropospheric ozone is discussed earlier in this report. The optimal goal (5% accuracy), is met by the IASI data in both lower and upper stratosphere in the mid-latitude. In the tropics and at high-latitude the accuracy is between 5 and 10% in the upper stratosphere, while for the lower stratosphere the accuracy is below 5%.

Table 3.2: ***Absolute differences (AD), relative Differences (RD) and standard deviation (STDEV) of IASI A, B and C ozone profile products versus ground-based reference profiles for lower and upper stratosphere and different latitude belts. Results are for the time period December 2019 – November 2020.***

	IASI A					
	Lower Stratosphere			Upper Stratosphere		
	AD (DU)	RD (%)	STDEV (%)	AD (DU)	RD (%)	STDEV (%)
Northern Polar Region	-9.0	-0.6	5.3	2.6	7.3	7.6
Northern Mid-Latitudes	1.7	3.5	6.5	1.9	3.3	4.5
Tropical Region	-1.6	-0.4	2.6	5.4	6.9	1.9
Southern Mid-Latitudes	3.8	2.7	5.4	1.8	3.4	4.5
Southern Polar Region	-	-	-	-	-	-
	IASI B					
	Lower Stratosphere			Upper Stratosphere		
	AD (DU)	RD (%)	STDEV (%)	AD (DU)	RD (%)	STDEV (%)
Northern Polar Region	-10.2	-1.2	5.8	2.4	6.7	7.7
Northern Mid-Latitudes	1.7	3.3	6.1	1.0	1.8	4.5
Tropical Region	-0.6	0.2	2.5	4.9	6.1	1.6
Southern Mid-Latitudes	3.1	2.3	5.6	2.0	3.6	4.6
Southern Polar Region	-	-	-	-	-	-
	IASI C					
	Lower Stratosphere			Upper Stratosphere		
	AD (DU)	RD (%)	STDEV (%)	AD (DU)	RD (%)	STDEV (%)
Northern Polar Region	-15.1	-3.0	5.5	2.2	5.6	6.4
Northern Mid-Latitudes	2.2	3.8	6.4	2.0	3.5	4.3
Tropical Region	-1.5	-0.2	2.4	5.6	7.0	2.0
Southern Mid-Latitudes	2.1	1.8	5.6	2.1	3.8	4.8

Southern Polar Region	-	-	-	-	-	-

4. Total ozone validation using ground-based measurements

The main aim of this section is to validate the IASI-MetopA (hereafter IASI-A), IASI-MetopB (hereafter IASI-B) and IASI-MetopC (hereafter IASI-B) total ozone column (TOC) products, processed with FORLI_v20151001, against the Dobson and Brewer spectrophotometer ground-based networks. In order to study the inter-sensor stability and consistency of the IASI measurements we directly compare them to the respective GOME2-MetopA (hereafter GOME-2A), GOME2-MetopB (hereafter GOME-2B) and GOME2-MetopC (hereafter GOME-2C) total ozone products. The retrieval algorithm is GDP4.8 for GOME2A and GOME2B, and GDP4.9 for GOME2C TOC.

4.1 Dataset description

4.1.1 IASI-A, IASI-B and IASI-C Total Ozone Columns

The IASI-A, IASI-B and IASI-C total ozone products shown in this report have been processed by EUMETSAT with the Fast-Optimal Retrievals on Layers for IASI Ozone (FORLI-O3) algorithm v20151001. Table 4.3 shows the main characteristics of the two satellite instruments. A full description of FORLI can be found in Hurtmans et al. (2012). An extensive validation of the IASI-A and IASI-B TOC retrieved with FORLI-O3 v20151001 is presented in Boynard et al. (2018), according to which:

- Both products were found to be consistent, with a global mean difference of less than 0.3 % for both daytime and night-time measurements; IASI-A being slightly higher than IASI-B.
- Concerning the validation results with respect to GOME-2 (Global Ozone Monitoring Experiment-2), Dobson, Brewer, SAOZ (Système d'Analyse par Observation Zénithale) and FTIR (Fourier transform infrared) TOCs, the global mean differences range between 0.1 % and 2 %. The maximum IASI discrepancies compared to all sources of TOC information (satellite and ground) were found at the southern high latitudes.

The IASI-A, IASI-B and IASI-C datasets were provided by EUMETSAT via FTP and cover the time period December 2019 – November 2020. The data files contain information for ozone profile, integrated ozone and other species, such as HNO_3, CH_4, CO, CO_2, N_2O and water vapor. For the purposes of the total ozone validation, only the integrated ozone was retrieved, along with other geophysical (i.e. solar zenith angle, latitude, longitude etc.) and influence quantities (i.e. surface and cloud information). According to the product's PUM (Product User Manual for the Near real-time IASI total O3 and O3 profile, Astoreca et al., 2020), the total ozone column is obtained by summing the partial columns on all retrieved layers.

Table 4.3: Main characteristics of the IASI-A, IASI -B and IASI-C instruments

Principle	**TIR Fourier transform spectrometer (Michelson interferometer with +/- 2 cm MOPD)**
Detectors	3 detectors corresponding to the 3 bands: Band I and II detectors are HgCdTe while band III is InSb type.
Spectral range	645 to 2760 cm^{-1}
Spectral resolution (FWHM)	0.5 cm^{-1} (apodized)
Spatial resolution	50 km x 50 km
Swath width	2200 km (±48.3°), 120 pixels
Eq. crossing time	09:30 & 21:30 LT ('tristar' configuration in a morning orbit)
Level-1-to-2 alg.	FORLI-O3 v20151001

Also, in the PUM, the quantity O3_QFLAG contained in the files is described as a single code assessing the quality of FORLI retrieved O3 total column and profiles. Its values can be equal to 2 (best quality), 1 (acceptable quality) or 0 (the rest):

- **O3_QFLAG=2** → the best quality pixels. It is noted that "this flag is not used for the moment, in the future will be a cost function".
- **O3_QFLAG=1** → for the valuable pixels, to use with caution. Calculated as using the following restrictions:
  - total cloud cover ≤13%
  - flags AMP_ERROR+AMP_EMPTY+AMP_INCOMPLETE+AMP_NEGPC + AMP_CONDITION+ AMP_DIVERGED +AMP_AVK are null (see Tables 3a and 3b)
  - RMS (residual rms) < 3.5e-8
  - -0.75e-9<BIAS (residual biased) < 1.25e-9
  - COL-06/COL TOT<0.085 (ratio of the partial column from ground to 6 km to the total column)
- **O3_QFLAG=0** for the remaining pixels, it is recommended not to be used.

The Product User Manual recommends that "only data with O3_QFLAG =2 should be used for validation or assimilation purposes, while if more pixels are needed, O3_QFLAG equal to 1 can be used but analysis must consider the not optimal quality of these pixels".

However, when overpass files for the locations of the ground-based stations were extracted from the IASI-A, -B and -C datasets, no pixels with O3_QFLAG=2 were found. The pixels with O3_QFLAG=1 were sparse, as it can be seen in Figure 4.11 (red pixels). It is calculated that for a specific mid-latitude ground-based station such as Thessaloniki, Greece, only 10% of the co-located (in space and in time) data have a quality flag equal to 1. Thus, it was decided not to use this particular flag for the filtering of the co-locations, since that would lead to an extremely limited dataset, not particularly useful for the validation of the total ozone product.

It is recommended that the description and recommended usage of the O3_QFLAG in the PUM is re-evaluated.

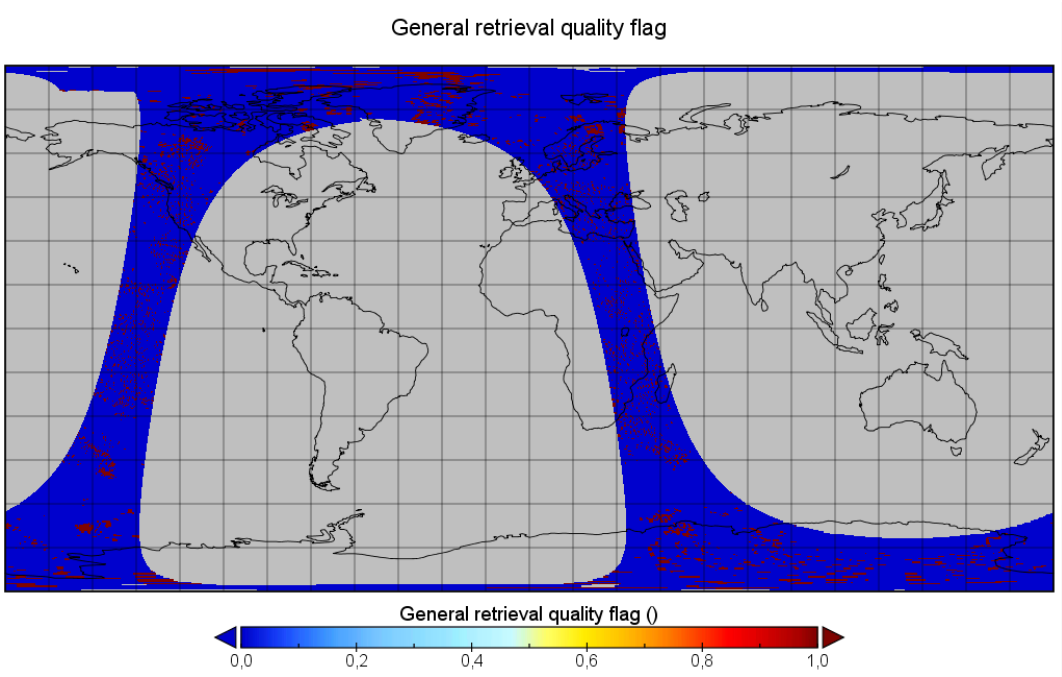

Figure 4.11: The General Retrieval Quality Flag (O3_QFLAG) parameter for an IASI-A orbit (72072), during 8th September 2020.

4.1.2 GOME2-MetopA, GOME2-MetopB and GOME2-MetopC

The temporally common total ozone columns measurements from GOME-2A, GOME-2B and GOME-2C were used to assess the consistency of IASI-A, IASI-B and IASI-C. The GOME2 TOCs were retrieved by the currently operational DOAS algorithm version GDP4.8 (GDP4.9 for GOME-2C) (ATBD, Valks et al., 2019). The total ozone products of the three sensors were

successfully validated, and their validation reports are published in Koukouli et al., 2015 and Garane et al., 2020.

In Table 4.4, the instrument characteristics of each GOME-2 instrument considered in the comparisons, are shown. Differences in the estimated total ozone can be a result of differences in the level-1 products, in the instruments and satellites themselves and therefore such differences should be considered when comparing two satellite datasets. The differential signal-to-noise characteristics of the instruments as well as the different degradation effects can have an impact on the total ozone column retrieval as well.

Table 4.4: Main characteristics of the GOME2A, GOME2B and GOME2C instruments

	GOME2/ MetopA	**GOME2/ MetopB**	**GOME2/ MetopC**
Principle	UV/VIS grating spectrometer		
Detectors	Reticon linear diode array		
Spectral resolution	0.26 nm		
Spatial resolution (default)	80 x 40 km^2 40 x 40 km^2 since July 15, 2013	80 x 40 km^2	80 x 40 km^2
Swath width	1920 km 960 km since July 15, 2013	1920 km	1920 km
Eq. Crossing time	09:30 LT		
Level-1-to-2 alg.	GDP 4.8	GDP 4.8	GDP 4.9

4.1.3 Ground-based total ozone observations

The ground-based measurements database used for this validation report consists of archived Brewer and Dobson total ozone data that are downloaded from the World Ozone and Ultraviolet Radiation Data Centre (http://www.woudc.org). WOUDC is one of the World Data Centers which are part of the Global Atmosphere Watch (GAW) program of the World Meteorological Organization (WMO). These data are quality controlled, first by each station before submission and secondly by WOUDC.

It is known that Dobson measurements suffer from a temperature dependence of the ozone absorption coefficients used in the retrievals which might account for a seasonal variation in the error of ±0.9% in the middle latitudes and ±1.7% in the Arctic, and for systematic errors of

up to 4% (Bernhard et al., 2005). The error of individual total ozone measurements for a well-maintained Brewer instrument is about 1% (e.g. Kerr, 1988). Despite the similar performance between the Brewer and Dobson stations, small differences within ±0.6% are further introduced due to the use of different wavelengths and different temperature dependence for the ozone absorption coefficients (Staehelin et al., 2003). Dobson and Brewer instruments might also suffer from long-term drift associated with calibration changes. Additional problems arise at solar elevations lower than 15°, for which diffuse and direct radiation contributions can be of the same order of magnitude.

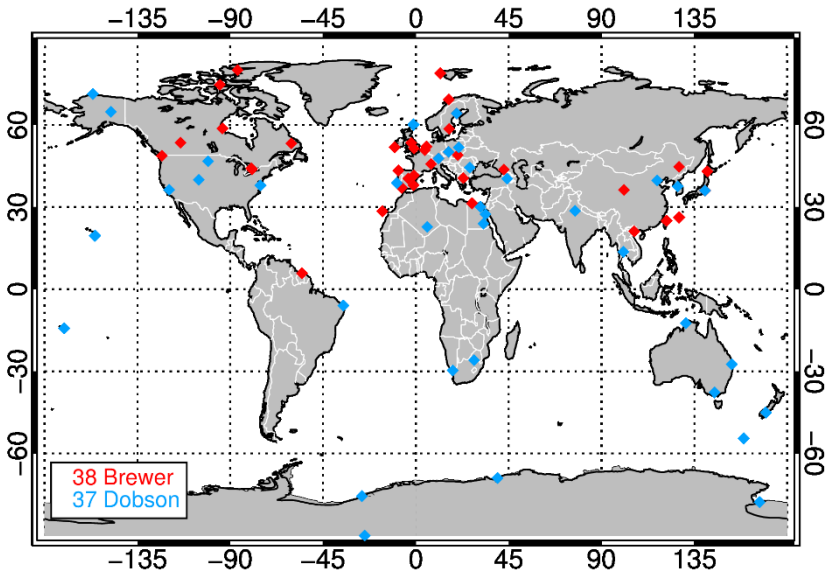

Figure 4.12: Spatial distribution of the Brewer and Dobson ground-based stations used for the comparisons.

To assure the quality of the reference ground-based data used for the validation of the IASI-A, IASI-B and IASI-C total ozone products, updated information were extracted from recent inter-comparisons and calibration records. This continuously updated selection of ground-based measurements has already been used numerous times in the validation and analysis of global total ozone records such as the inter-comparison between the OMI/Aura TOMS and OMI/Aura DOAS algorithms (Balis et al., 2007a), the validation of ten years of GOME/ERS-2 ozone record (Balis et al., 2007b), the validation of the updated version of the OMI/Aura TOMS algorithm (Antón et al., 2009), the GOME-2/MetopA validation (Loyola et al., 2011; Koukouli et al., 2012), the GOME-2/MetopB validation (Hao et al., 2014), the evaluation of the European Space Agency's Ozone Climate Change Initiative project (O3-CCI) TOCs (Koukouli et al., 2015, Garane et al., 2018) and the validation of the TROPOMI/S5P total ozone products (Garane et al., 2019). In all the aforementioned publications, LAP/AUTH assumes the leading role in the validation efforts.

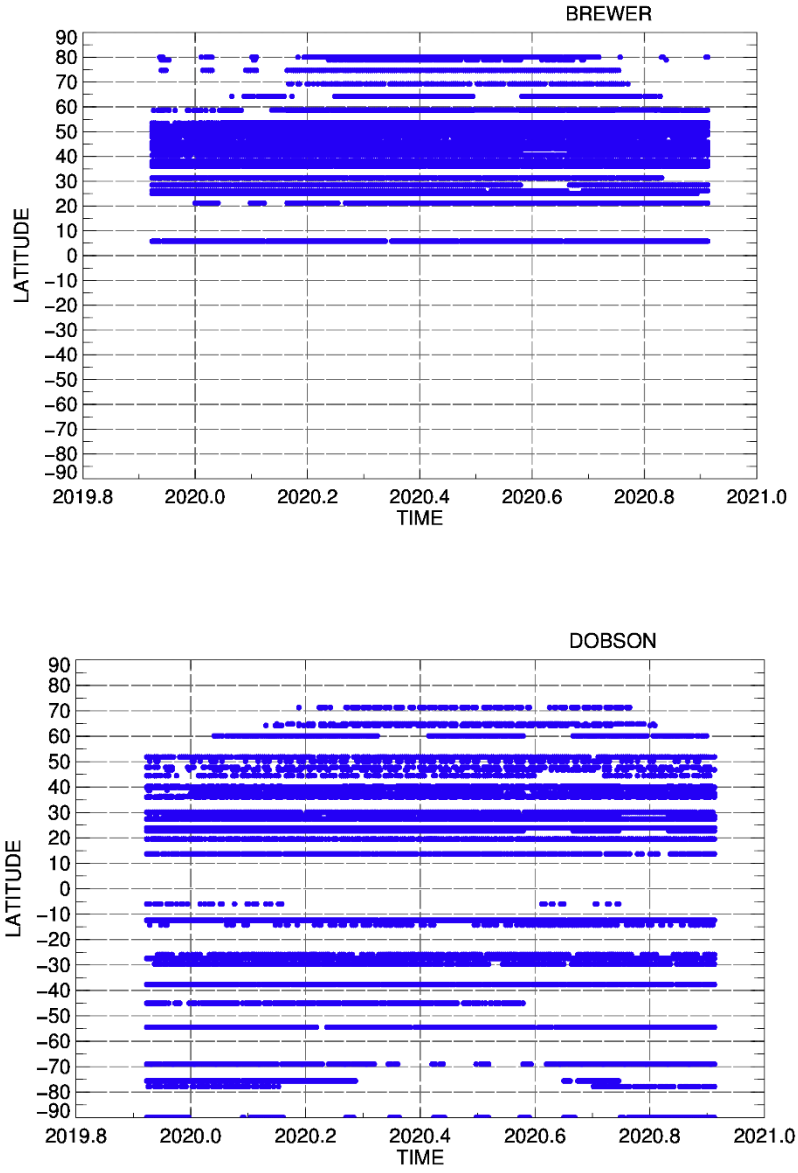

Figure 4.13: Spatial and temporal representation of the co-location data used for the validation with ground-based measurements (upper panel: Brewer, lower panel: Dobson) for the time period December 2019 to November 2020.

In this report, archived data for the period December 2019 to November 2020 are used for the comparisons, depending on the availability of data for each individual station. The Brewer and Dobson WOUDC stations considered for the comparisons are listed in Tables A.1 and A.2 (Appendix 1) and their geographical distribution is depicted in Figure 4.12. In Figure 4.13, the spatio-temporal distribution of the co-locations of the ground-based measurements is shown.

In the comparison plots and statistics presented in this report, only the direct sun observations provided by the Brewers and Dobsons are utilized for the computation of the percentage differences between satellite and co-located (in space and in time) ground-based measurements, since they are considered of higher accuracy than all the other types of ground-based observations. Finally, only northern hemisphere Brewer ground-based stations are considered, because the number of stations in the southern hemisphere is very limited and they are mainly located in Antarctica.

4.2 Validation results of IASI-A, IASI-B and IASI-C total ozone with respect to ground-based measurements

In this section, the archived and quality-controlled Dobson and Brewer daily total ozone measurements downloaded from WOUDC for the period December 2019 to November 2020, are used as ground-truth for the validation of IASI-A, IASI-B and IASI-C total ozone measurements. The datasets of the three satellite sensors are temporally and spatially co-located to ground-based measurements using the following co-location criteria:

- the satellite and daily ground-based total ozone measurements must correspond to the same day, and
- the maximum search radius between the ground-based stations and the centre coordinates of the satellite pixel is set to 50 km. The spatially closest satellite observation is paired with the ground-based station's daily-mean measurement.

This is an established methodology followed in many total ozone validation reports in the past (either for integrated ozone profiles or for the operational products), as well as in numerous published papers for total ozone column validation (for example, Koukouli et al., 2015; Garane et. al. 2018; Garane et. al, 2019; Garane et al., 2020).

The pairs of co-located satellite and daily-mean ground-based measurements are used to calculate their percentage difference by the simple formula:

$$Diff\ (\%) = \frac{(satellite - ground)}{ground}\%$$

The datasets of percentage differences were not filtered by any parameter.

In all plots that also contain an error bar this represents the 1-σ, i.e. the standard deviation on the mean percentage differences. The mean values are always extracted from averaging all individual daily co-locations that fall within the bin in question. The monthly mean values were calculated from the total number of available co-locations per month.

For the purposes of this validation report, in Section 4.4 only the temporally common co-locations to ground-based measurements between the GOME-2A, GOME-2B and GOME-2C are used to achieve the comparability between the datasets, i.e. between December 2019 and November 2020.

4.2.1 IASI-A TOC validation with respect to ground-based observations

The percentage differences of the IASI-A and co-located (in space and in time) ground-based total ozone column observations are used in the histograms (left panels) and the scatter plots (right panels) seen in Figure 4.14. The Brewer co-locations are shown in the upper panels of the figure and the Dobson co-locations in the bottom panels. The overall agreement between IASI-A and the ground-based TOCs is excellent, their correlation coefficient being greater than 0.94. The mean relative bias between satellite and ground-based TOCs is 0.19% for the Brewer comparisons and 0.14% for the Dobson co-locations, indicating that IASI-A reports slightly higher TOCs. The mean standard deviation of the percentage differences is about 4.5%, which also includes the variability of the ground-based measurements and any possible co-location mismatch.

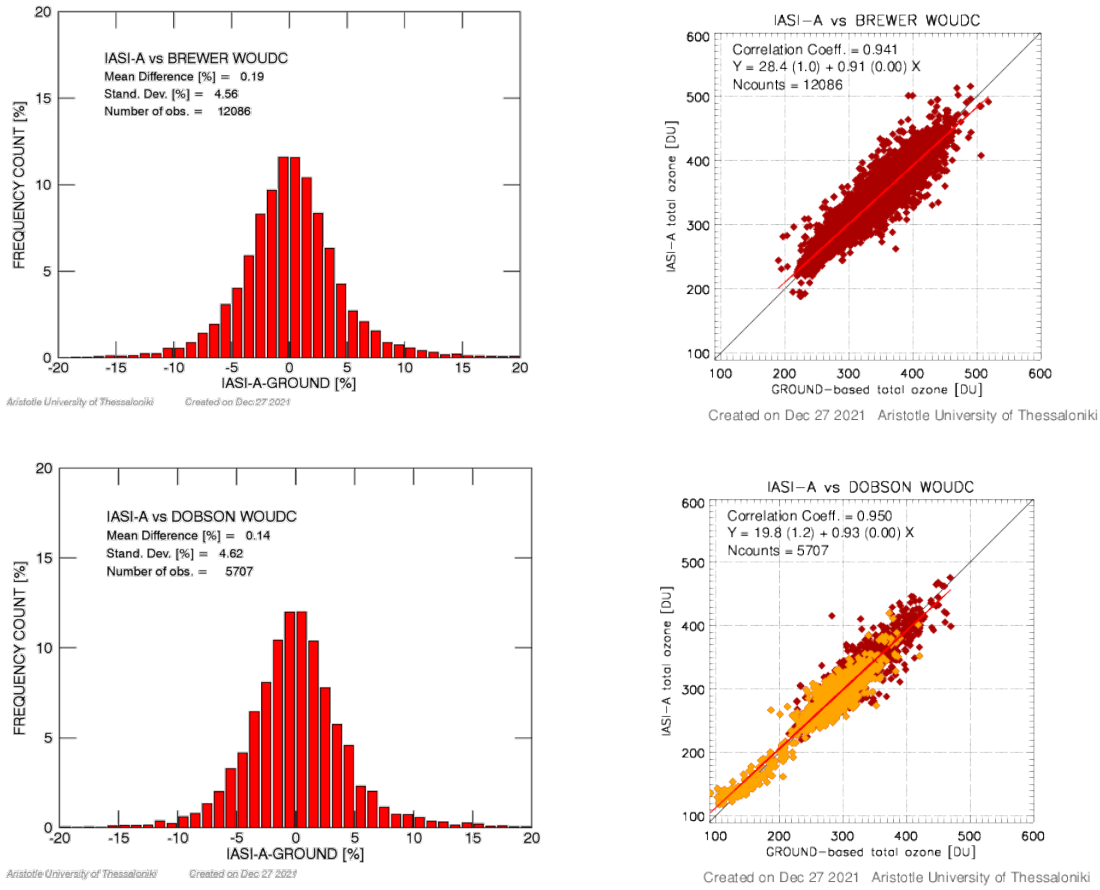

Figure 4.14: The histograms (left panels) and the scatter plots (right panels) of the comparisons between the co-located total ozone columns retrieved by IASI-A and ground-based measurements (upper panels: Brewer, bottom panels: Dobson). The yellow points in the bottom right panel show the Dobson and IASI-A co-locations at the southern hemisphere.

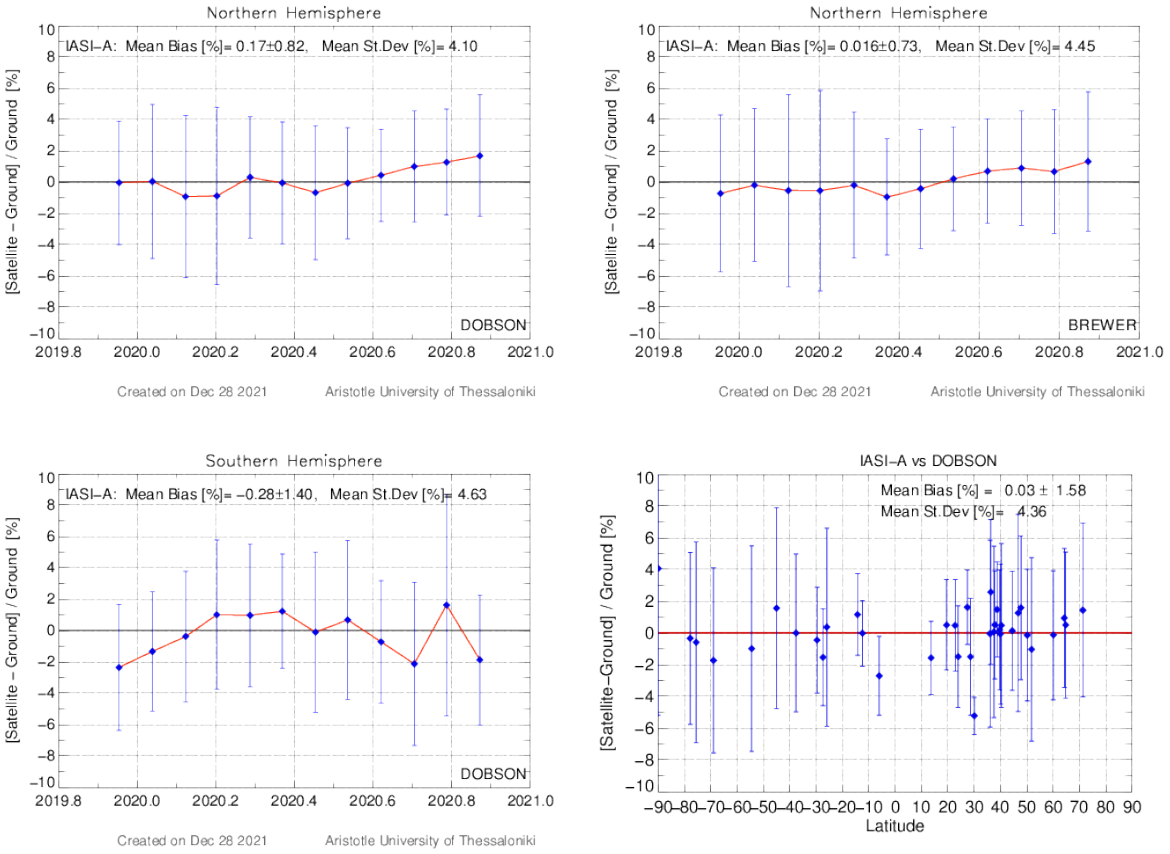

Figure 4.15: Left panels and the upper-right panel show the hemispherical monthly mean percentage differences between IASI-A and ground-based TOCs (upper-left: northern hemisphere with respect to Dobson, bottom left: southern hemisphere with respect to Dobson and upper-right: northern hemisphere with respect to Brewers). Bottom-right panel shows the mean relative bias for each Dobson station with respect to the station's latitude.

Figure 4.15, left panels and the upper-right panel, show the hemispherical monthly percentage differences between IASI-A and ground-based TOCs. The northern hemisphere comparisons with respect to Dobsons are shown at the upper-left panel, the bottom left panel shows the southern hemisphere comparisons with respect to Dobson observations and the upper-right panel presents the northern hemisphere comparisons with respect to Brewer measurements. The seasonal variability of the comparisons cannot be studied due to the limited temporal range of the dataset, nevertheless a common feature seen both in the Dobson as well as in the Brewer time-series is the increase in the mean bias since June 2020 until November 2020, by ~2.5%. This could be a seasonal effect, but due to the limited dataset it cannot be said with certainty. The overall northern hemisphere mean bias ranges between -0.3% and 0.2%, showing a very good agreement between the two datasets, satellite and ground-based, irrespective of time.

The bottom-right panel of Figure 4.15 shows the mean relative bias and standard deviation for each Dobson station with respect to the station's latitude. The number of stations with available co-locations in the southern hemisphere is smaller compared to the northern hemisphere. All stations have a mean bias within ±2% with very few exceptions, like Amundsen-Scott, Antarctica, at 90°S, which shows a mean bias of +4%. The deduction of an increased overestimation of TOC by IASI-A would be firmer if more ground-based stations were available in this area or a longer satellite dataset. On the other hand, the same overestimation was also seen in Boynard et al., 2018. In that work, a longer time series was available and four Antarctic stations were studied. It was seen that the overestimation, mainly present in Amundsen-Scott, was due the IASI total ozone observations, and their potential need for additional quality filters, e.g., on ice surface emissivity issues. The algorithm used in the total ozone retrieval was also FORLI v20150101, therefore this conclusion applies here as well.

4.2.2 IASI-B TOC validation with respect to ground-based observations

Figure 4.16 shows the histograms (left panels) and the scatter plots (right panels) for the IASI-B co-locations compared to the respective ground-based Brewer (upper panels) and Dobson stations observations (bottom panels). The agreement between satellite and ground-based observations is excellent, with a correlation coefficient of 0.94 – 0.95. The overall mean bias is 0.2 - 0.3 %, showing a marginal overestimation of total ozone by IASI-B. Finally, the standard deviation is 4.5%, very similar to the IASI-A comparisons.

The hemispheric monthly mean time series shown in Figure 4.17, left panels for the Dobson comparisons and upper right panel for the Brewer co-locations, have almost the same patterns as those seen for IASI-A (Figure 4.15). The mean bias per hemisphere is also very similar to IASI-A, ranging between -0.2 % (Dobson stations at the southern hemisphere) and 0.4% (Dobson, northern hemisphere).

Figure 4.17, bottom right panel, shows the mean bias and the respective standard deviation per station for the Dobson network. All stations have a mean bias within ±2% with the Amundsen-Scott being the only exception, at +3%. The reason for this high bias was explained in section 4.2.1.

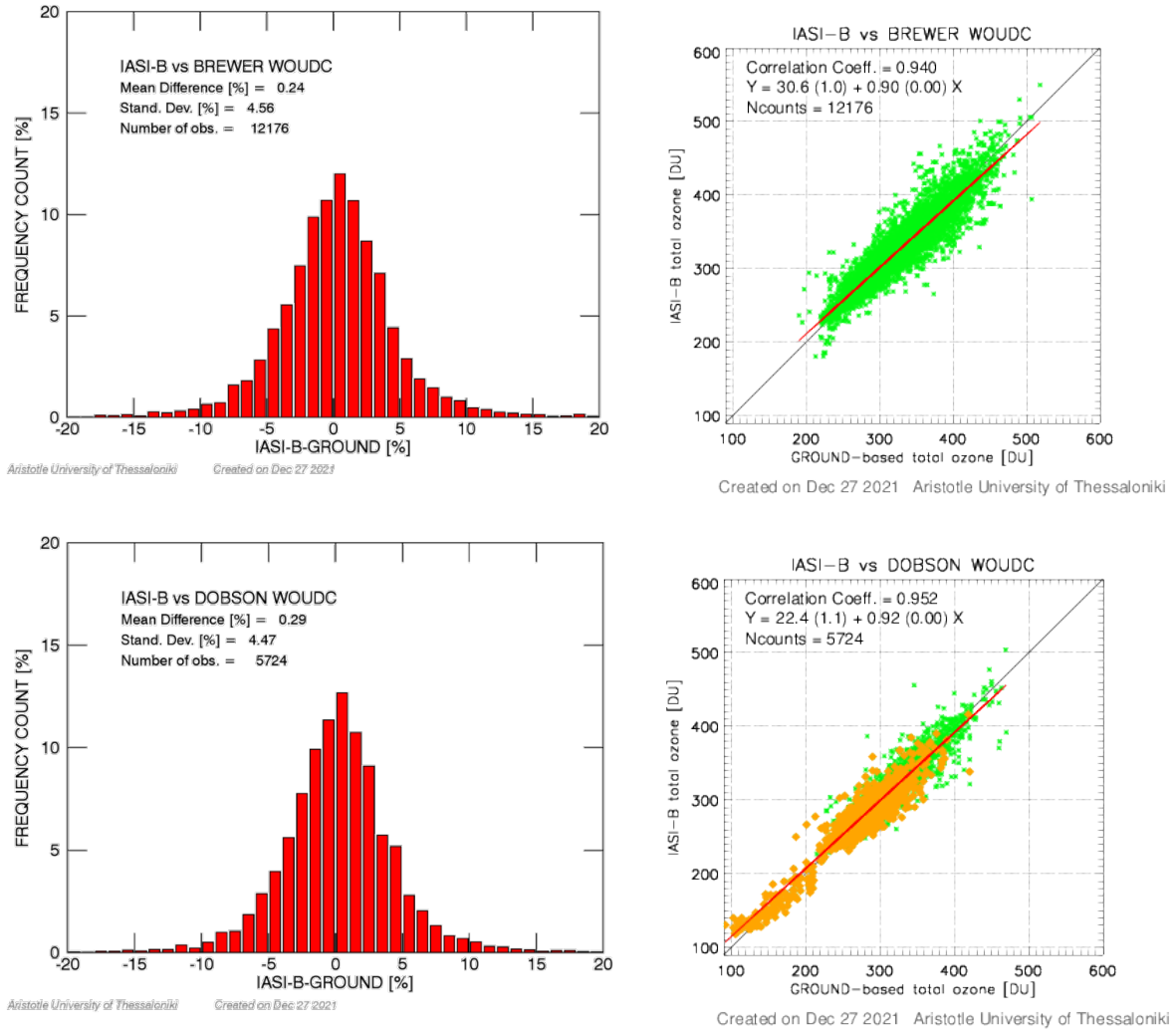

Figure 4.16: As in Figure 4.14 for IASI-B.

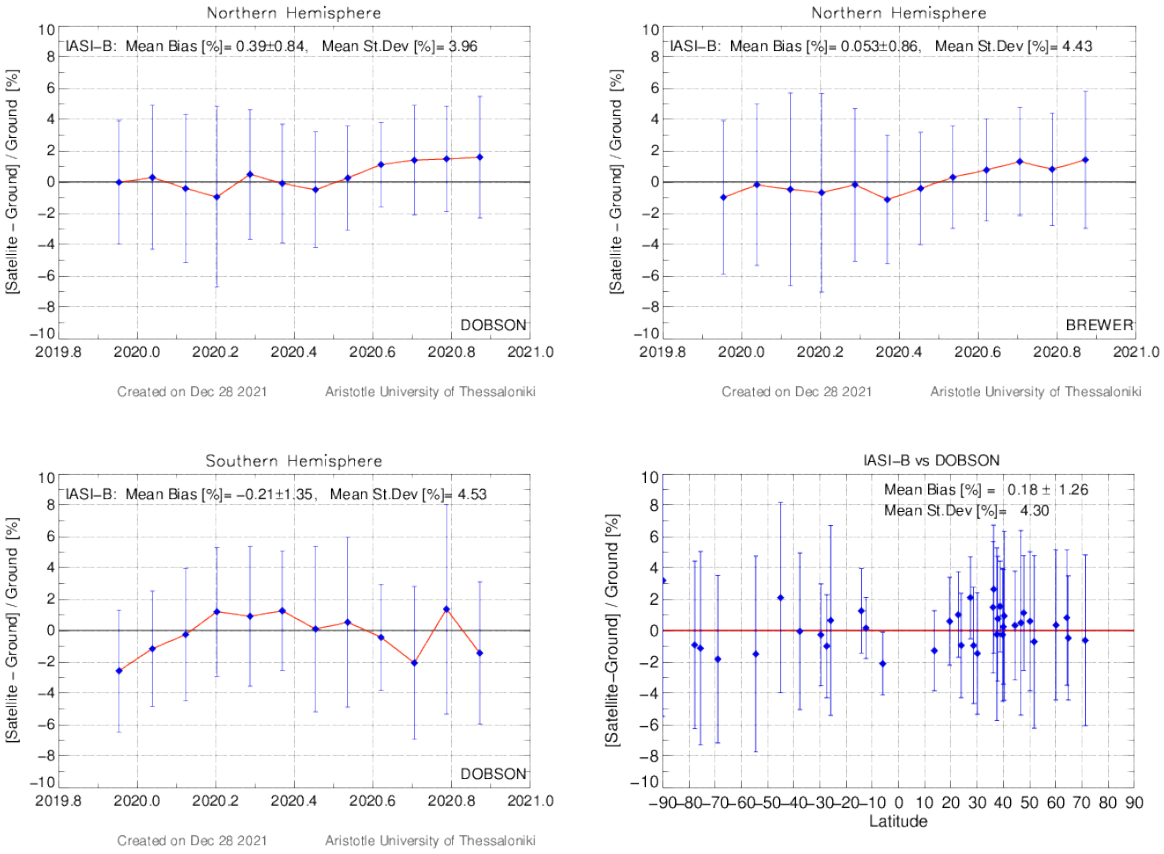

Figure 4.17: As in Figure 4.15 for IASI-B

4.2.3 IASI-C TOC validation with respect to ground-based observations

The same analysis is performed for the IASI-C co-locations to ground-based TOC observations. Figure 4.18 shows the shows histograms (left panels) and the scatter plots (right panels) for the IASI-C comparisons with respect to ground-based Brewer (upper panels) and Dobson stations observations (bottom panels). The agreement between satellite and ground-based observations is again very good, with a correlation coefficient of 0.94 – 0.95. The overall mean bias is 0.5 - 0.7 %, showing a slight TOCs overestimation by IASI-C. Finally, the standard deviation is again 4.5%.

The patterns of the hemispheric monthly mean time series shown in Figure 4.19 (left panels for the Dobson comparisons and upper right panel for the Brewer co-locations), are almost the same as those seen for IASI-A (Figure 4.15) and IASI-B (Figure 4.17). The mean bias per hemisphere is slightly higher compared to IASI-A and IASI-B, ranging between 0.2 % (Dobson stations at the southern hemisphere) and 0.7% (Dobson, northern hemisphere).

Finally, Figure 4.19 bottom right panel, shows the mean bias and the respective standard deviation per station for the Dobson network. Most stations have a mean bias within ±2% with

the Amundsen-Scott being the only exception, at 3%. The reason for this high bias is explained in section 4.2.1.

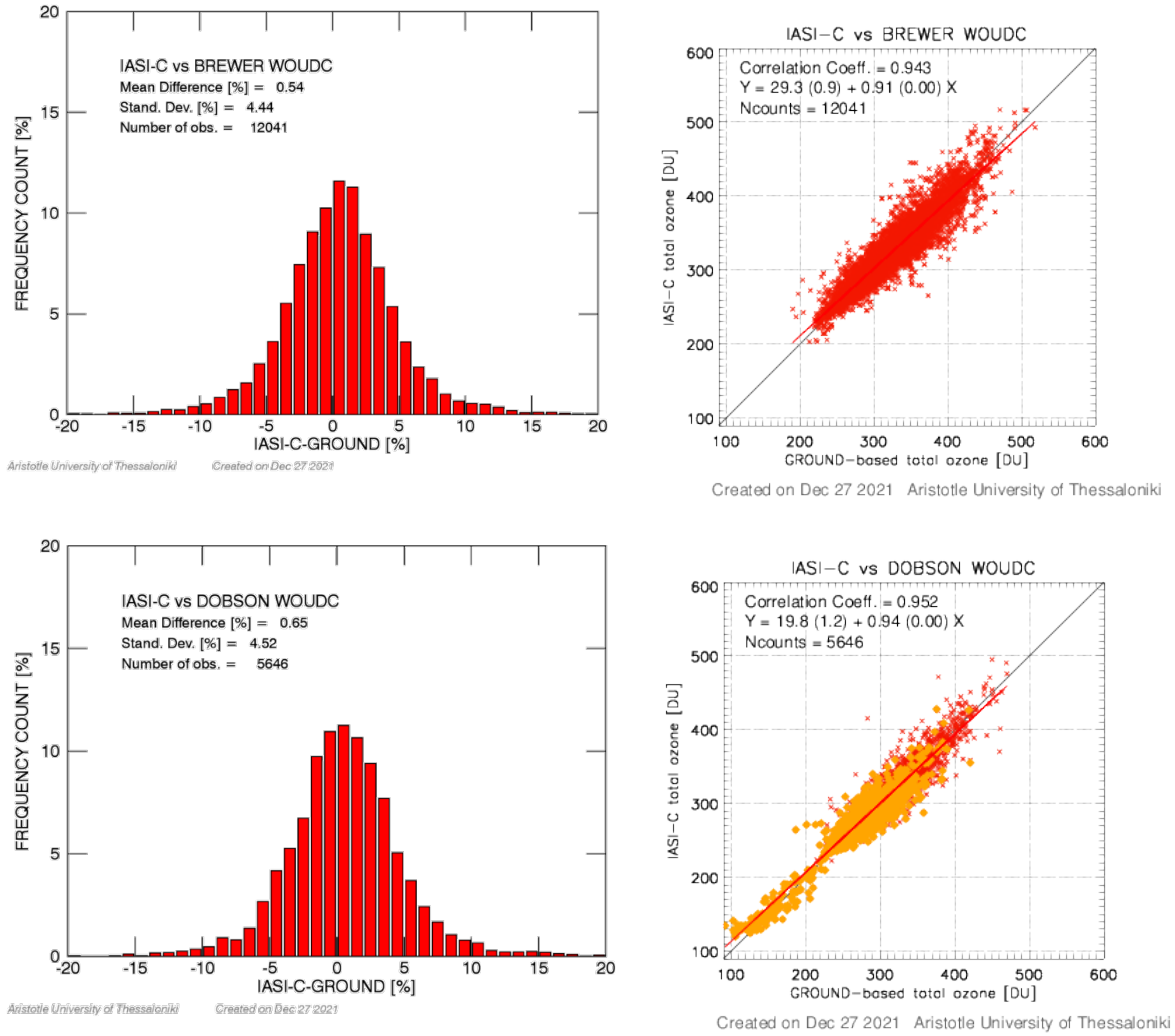

Figure 4.18: As Figure 4.14 for IASI-C

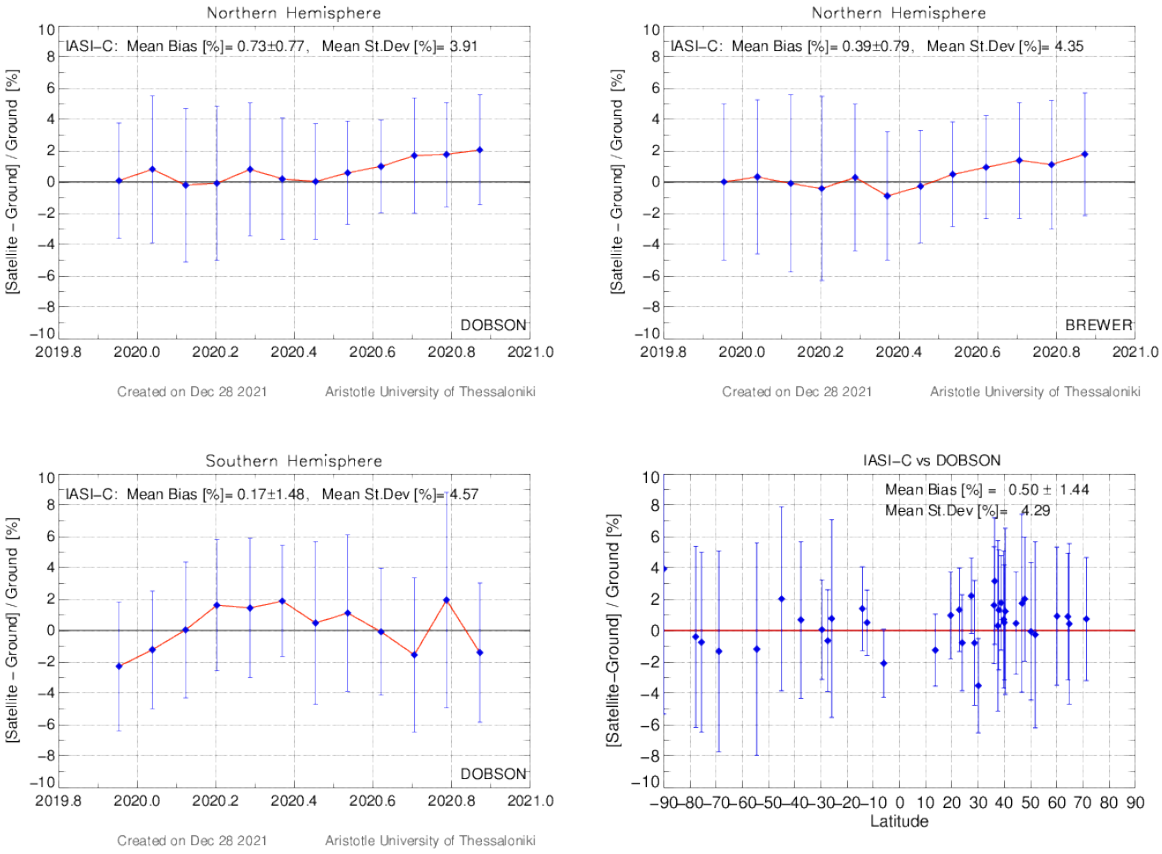

Figure 4.19: As Figure 4.15 for IASI-C.

4.3 IASI-MetOpA, IASI-MetOpB and IASI-MetOpC consistency checks via their co-located comparisons to Brewer & Dobson instruments

In this section, the validation results of IASI-A, IASI-B and IASI-C with respect to their co-located ground-based total ozone observations are inter-compared in order to examine the consistency of the three sensors.

In Figure 4.20, the latitudinal dependency of the three satellite instruments comparisons with respect to their co-located ground-based observations (Dobson left panel, Brewer right panel), is shown. IASI-A is depicted with blue symbols and line, IASI-B with green symbols and line and IASI-C with red symbols and line. Dobson ground-based measurements are used in the left panel and Brewer in the right panel. In this figure, the co-locations of all stations are averaged in 10° latitude bins and their means and standard deviations per latitude bin are shown. First, it is evident from both panels that the consistency between the three sensors is excellent, varying within ±1% for most latitude bins. The variability (standard deviation of the means) is also very similar. The mean bias for all latitude bins is within 0 to 2% for the Brewer comparisons, while the southern hemisphere Dobson co-locations have a higher variability in mean bias due to the limited number of stations in this part of the earth. Nevertheless, the low bias in the latitude bin 0 to -10°S and the higher bias in the bin -40°S to -50°S is a feature that is frequently seen in many validation exercises and can be attributed to the Dobson ground-based network. The quite higher mean bias at the -80° to -90° latitude bin, containing only the Amundsen-Scott station, is a common feature for all IASI sensors, that was discussed in section 4.2.1.

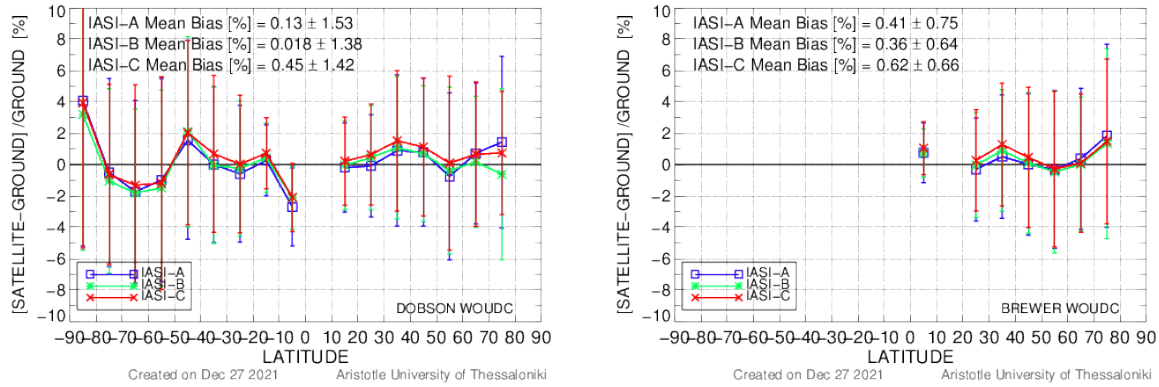

Figure 4.20: The latitudinal dependency of the IASI-A (blue symbols and line), IASI-B (green symbols and line) and IASI-C (red symbols and line) comparisons to Dobson (left panel) and Brewer (right panel) ground-based measurements. The ground-based stations are averaged in 10° latitude bins.

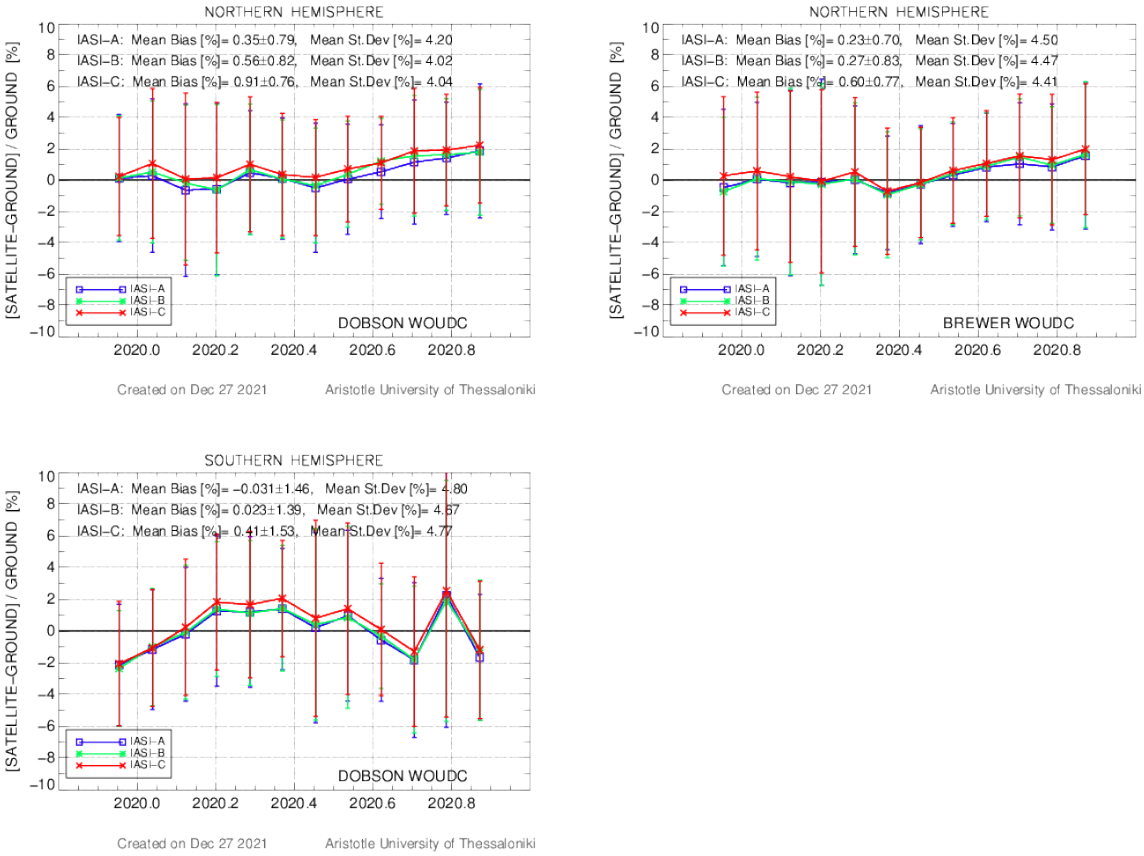

Figure 4.21: The hemispheric time series of the monthly mean relative bias of the Dobson co-locations (northern hemisphere: upper left panel, southern hemisphere: bottom left panel) and Brewer comparisons (right panel). The three sensors (IASI-A, IASI-B and IASI-C) are shown with different line and symbol colours.

Figure 4.21 shows the hemispheric time series of the monthly mean relative bias for the three sensors, IASI-A, IASI-B and IASI-C following the same colour code. The Dobson comparisons are shown to the left panels (upper: northern hemisphere, bottom: southern hemisphere) and the Brewer co-locations are used for the right panel. The temporal agreement between the three satellite instruments is exceptional, ranging from ~0% to ~ 1%. Some months in the southern hemisphere have a higher standard deviation but this introduced by the ground-based observations.

Influence quantities

In this section, a number of parameters that play a key role in the total ozone retrieval by the FORLI algorithm, will be investigated.

i. Solar zenith angle

Figure 4.22 shows the dependence of the percentage differences between satellite and ground-based co-located total ozone observations on solar zenith angle (SZA). All sensors are very stable for SZAs within 30° and 70°, but appear to deviate for higher angles, where the number of co-locations is smaller and the measurement uncertainty is higher. The agreement between the three sensors for SZAs lower than 70° is within 1.5%, with IASI-C showing higher discrepancies with respect to the ground-based total ozone measurements than the other two sensors. The Brewer comparisons (right panel) show increased percentage differences for SZAs between 20° and 30°, but the number of co-locations, especially below 25°, is very limited.

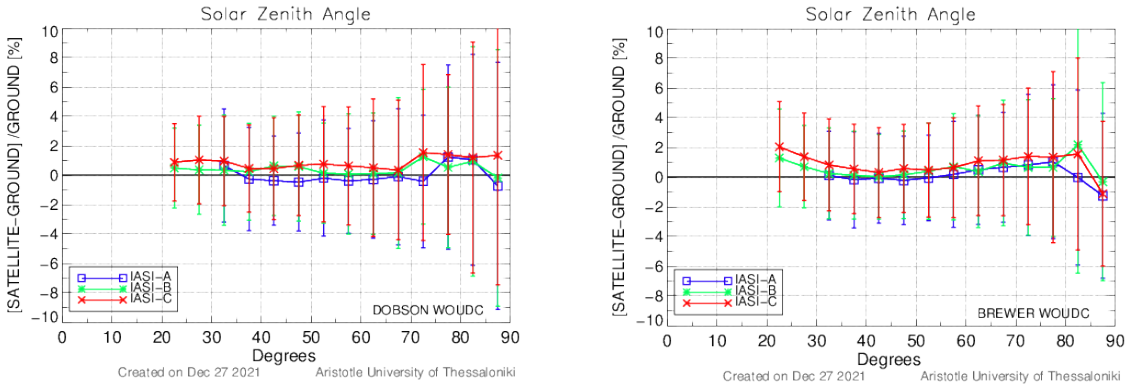

Figure 4.22: The dependence of the percentage differences between satellite and ground-based observations (left Dobson, right Brewer), on solar zenith angle. As above, three sensors (IASI-A, IASI-B and IASI-C) are shown with different line and symbol colours.

ii. Clouds

According to the FORLI v20151001 ATBD, the cloud fraction input parameter, which is very important for the total ozone retrieval, is a criterion based on which some pixels are not processed at all: "Only pixels with a cloud fraction equal to or lower than 13 % are processed".

However, the IASI datasets that were provided from EUMETSAT for all three sensors contain pixels with cloud fraction > 13%. These pixels would be filtered out of the co-location dataset if the rule of O3_QFLAG =1 was applied. But, as it was analyzed in section 4.1.1, for this validation report it was chosen not to apply this filter, since the resulting number of co-locations would not be enough to lead the study to solid conclusions about the quality of the IASI-A, IASI-B and IASI-C total ozone product.

In Figure 4.23, the dependence of the percentage differences on Cloud Fraction (in %, upper left panel), Cloud Top Pressure (in hPa, upper right panel) and the Cloud Top Temperature (in K, bottom panel) is depicted for the three sensors when compared to Dobson observations. The numbers at the top of the plots mean that for the particular bin where they appear the data point resulted from averaging a very limited number of co-locations, less than 3% of the total.

Therefore, these averaging bins should be treated with caution. It is evident, that there is no significant dependence on the cloud parameters for any of the three sensors. The respective figures based on the Brewer co-locations are shown in Appendix II.

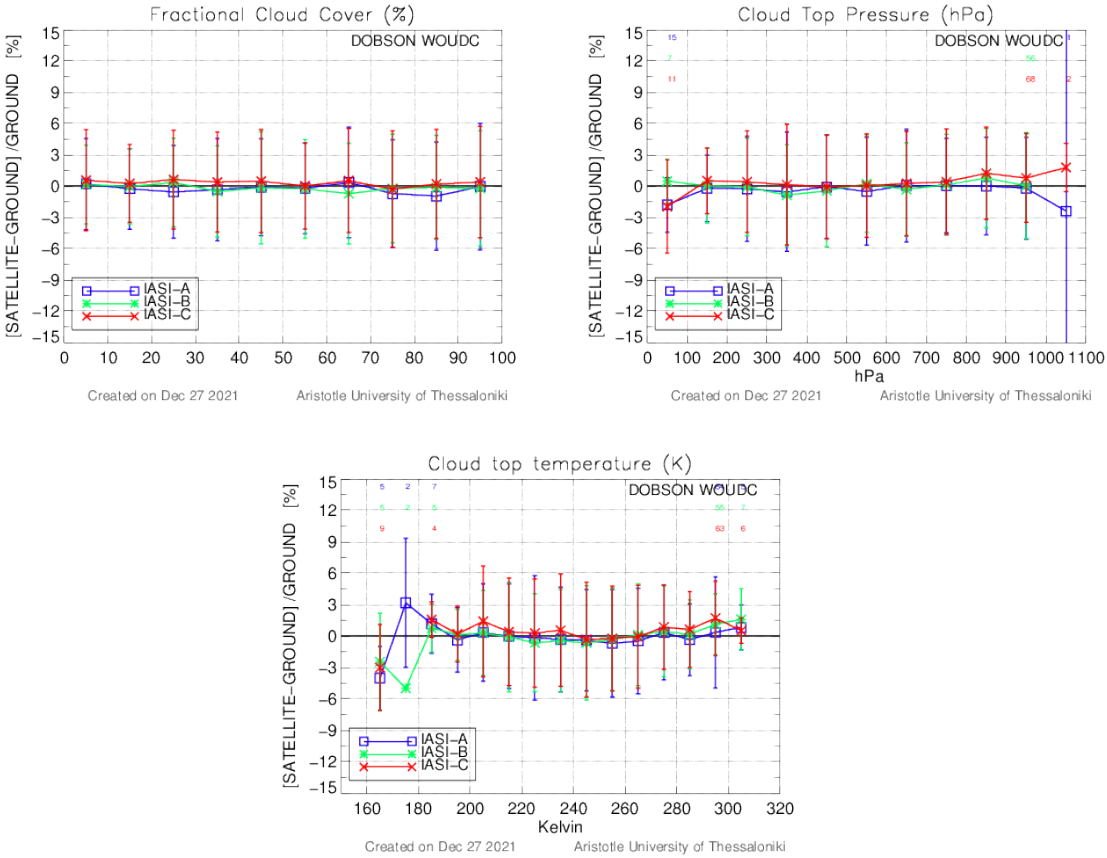

Figure 4.23: The dependence of the percentage differences between satellite and Dobson ground-based observations, on Cloud Fraction (in %, upper left panel), Cloud Top Pressure (in hPa, upper right panel) and the Cloud Top Temperature (in K, bottom panel). Again, the three sensors (IASI-A, IASI-B and IASI-C) are shown with different line and symbol colours.

iii. Surface properties

Finally, in Figure 4.24 the dependence of the percentage differences between satellite and Dobson ground-based observations, on Surface Altitude (in m, upper left panel), Surface Temperature (in K, upper right panel) and Surface Pressure (in hPa, bottom panel), is shown for all three sensors (IASI-A, IASI-B and IASI-C). As already mentioned in the previous paragraph, the averaging bins with numbers on top of the plot should be treated with caution.

Thus, based on the plots in Figure 4.24 it can be deduced that there is no important dependency on surface altitude. The increased bias for the bin 2.6 km – 2.8 km is due to the contribution of the Amundsen-Scott ground-based observations. The surface pressure parameter does not affect the total ozone comparisons, either. The same is also true for the surface temperature dependency, for temperatures above 260K. Below that point the bias of the three sensors is 2-3%, meaning that IASI overestimates total ozone when the surface temperatures is that low. The overestimation becomes about 20% for temperatures 210-220K and 40% when the temperatures are even lower, 200-210K. Obviously these co-locations correspond to stations located in Antarctica.

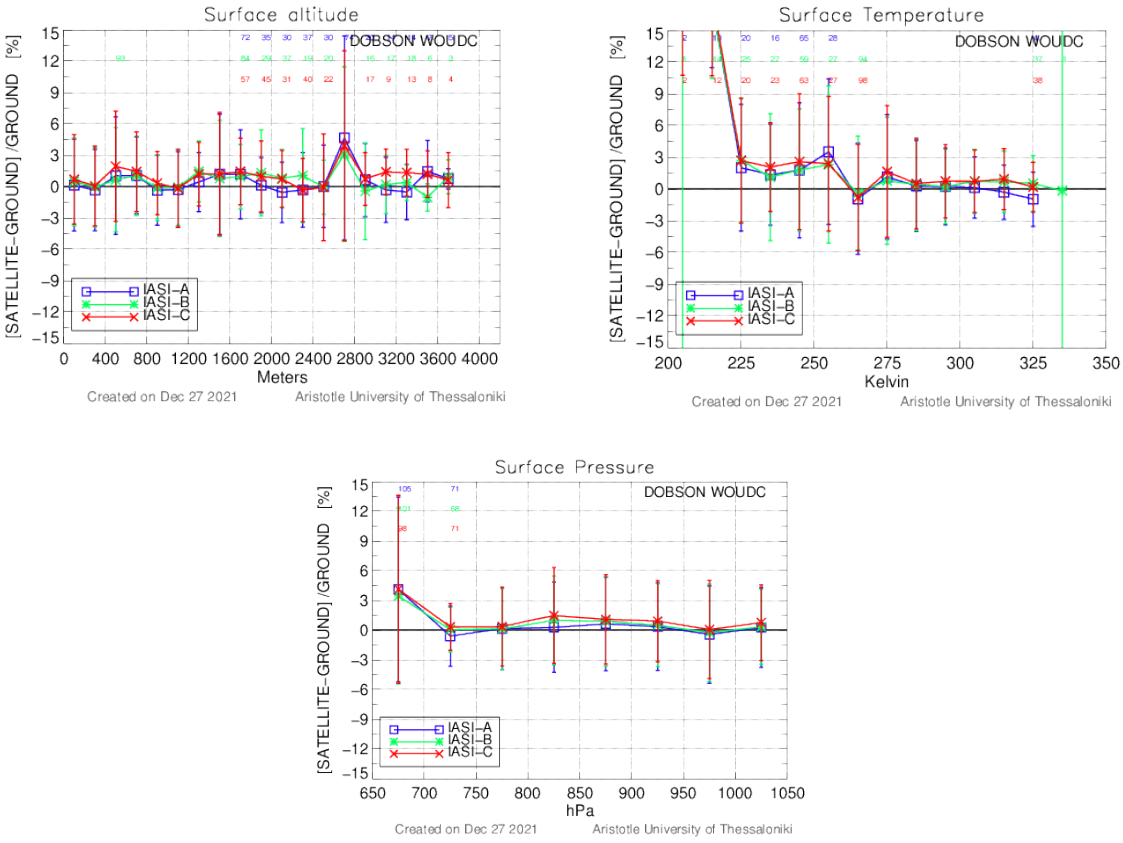

Figure 4.24: The dependence of the percentage differences between satellite and Dobson ground-based observations, on Surface Altitude (in m, upper left panel), Surface Temperature (in K, upper right panel) and Surface Pressure (in hPa, bottom panel). The three sensors (IASI-A, IASI-B and IASI-C) are shown with different line and symbol colours.

4.4 IASI-A, -B and -C consistency checks with respect to GOME2-A, -B and -C via their co-located comparisons to Brewer & Dobson instruments

In this section, IASI-A, IASI-B and IASI-C are indirectly compared to GOME-2A, GOME-2B and GOME-2C, respectively, via their co-locations to ground-based observations performed by Brewer and Dobson instruments. To achieve the best possible comparability between the IASI and GOME-2 co-location datasets, they were inter-compared and only temporally common co-locations for the two types of instruments were used.

Figure 4.25, Figure 4.26 and Figure 4.27, show the percentage differences between satellite (IASI-A, IASI-B and IASI-C respectively) and ground-based Dobson TOC measurements, in the form of:

- hemispheric time series for the northern hemisphere (upper left panel) and for the southern hemisphere (bottom left panel),
- latitudinal dependency (upper right panel) and
- the dependence on SZA (bottom right panel).

The blue line and symbols correspond to IASI co-locations and the red line and symbols show the GOME-2 comparisons to ground-based instruments. The respective plots against Brewer ground-based observations are shown in Appendix II.

Table 4.5 Summary table showing the mean bias (in %) and standard deviation (1σ) of the IASI and GOME-2 comparisons to Dobson and Brewer ground-based measurements.

	Dobson		Brewer
	NH Mean Bias	**SH Mean Bias**	**NH Mean Bias**
IASI-A	+0.3 ± 0.9 %	-0.2 ± 1.4 %	+0.3 ± 0.8 %
GOME-2A	+0.6 ± 0.6 %	0.7 ± 2.8 %	+1.0 ± 0.8 %
IASI-B	+0.6 ± 0.8 %	-0.0 ± 1.3 %	+0.3 ± 0.8 %
GOME-2B	+1.4 ± 1.2 %	+0.7 ± 1.5 %	+1.6 ± 1.1 %
IASI-C	+1.0 ± 0.7 %	+0.3 ± 1.4 %	+0.6 ± 0.8 %
GOME-2C	+2.3 ± 0.6 %	+1.7 ± 1.3 %	+2.4 ± 0.6 %

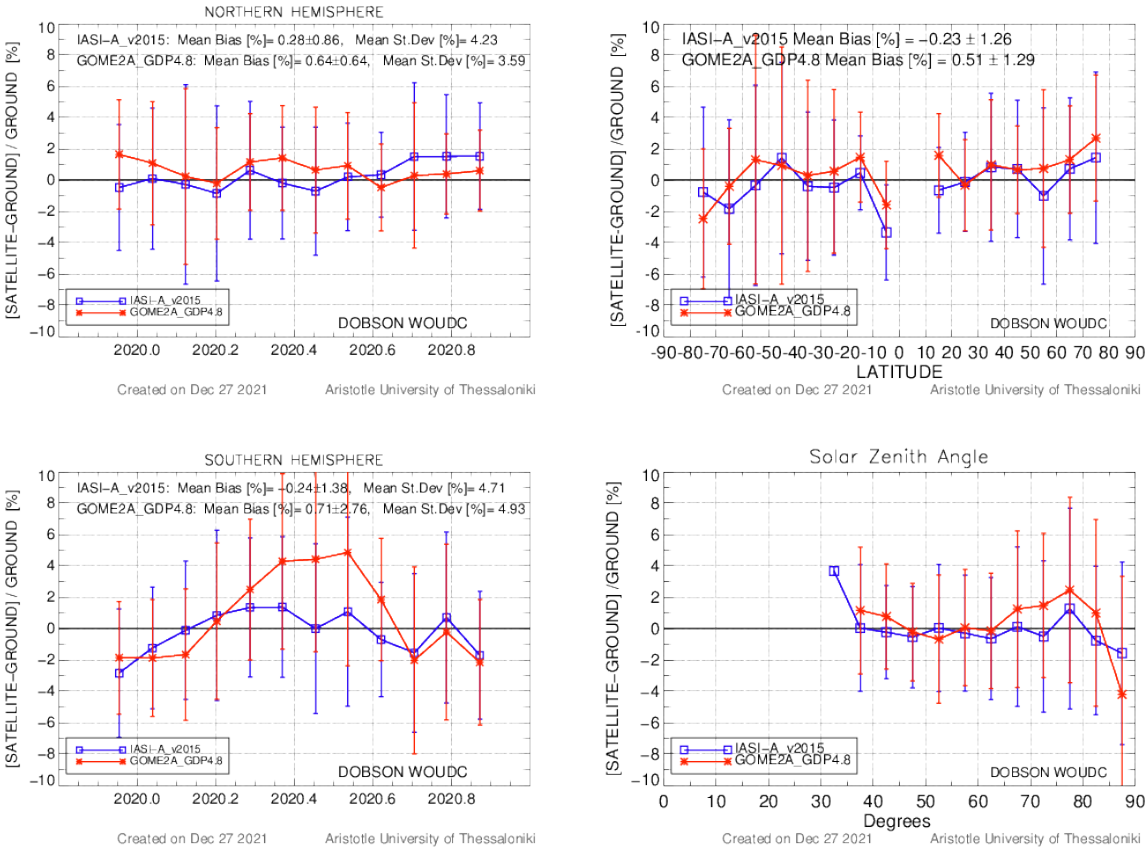

Figure 4.25: The percentage differences between satellite and ground-based Dobson TOC measurements, in the form of hemispheric time series for the northern hemisphere (upper left panel), for the southern hemisphere (bottom left panel), latitudinal dependency (upper right panel) and the dependence on SZA (bottom right panel). The sensors seen in the plots are IASI-A (blue line and symbols) and GOME-2A (red line and symbols).

Regarding the difference in mean bias between the two satellite sensors, it is seen in the summary Table 4.5 that GOME-2 reports higher TOCs with respect to IASI, by ~ 0.5% for MetOpA, ~1% for MetOpB and ~1.5% for MetOpC. As for the temporal stability of the monthly mean bias between the IASI and GOME-2, all sensors except for GOME-2A in the southern hemisphere have a comparable standard deviation of the mean (1σ) of about 1%. During the 2019-2020 winter months and since July 2020 GOME-2A was switched to an empirical model due to loss of solar visibility, therefore the inter-comparison of IASI-A and GOME-2A should be handled with caution. The difference between IASI-B and GOME-2B (Figure 4.26) is lower during summer of each hemisphere, about 0 to 1%, and goes up to 3% for the available winter months of this dataset. GOME-2C is known to record higher total ozone values than GOME-2B by about 0.5% (Garane et al., 2020), which is also reflected in Figure 4.27, where IASI-C is constantly below the GOME-2C curve in the best populated northern hemisphere, with their difference ranging between 0.5 to 2%.

The latitudinal dependence of IASI is also very similar to GOME-2, as shown in the right upper panels of Figures Figure 4.25, Figure 4.26 and Figure 4.27. Maximum divergencies between the two sensors are seen for the latitude bins -50°S to -70°S, where a very limited number of ground-based stations is available. For the northern hemisphere, the comparisons are excellent for the latitude bins 20°N - 60°N, within 1.5% for IASI-B and GOME-2B, and a little higher for IASI-C and GOME-2C, up to 2%.

As for the dependence of the satellite to ground-based percentage differences on solar zenith angle, the bottom right panels of Figures Figure 4.25, Figure 4.26 and Figure 4.27 show that for the co-locations with SZAs below 50° IASI-A and IASI-B is in excellent agreement to GOME-2A and GOME-2B, respectively, within 0.5%. Their difference in mean bias increases up to 2.5% for SZAs above 60°. IASI-C has the same deviation with respect to GOME-2C above 60°, but below that angle there is a divergence increasing with SZA, up to ~2%.

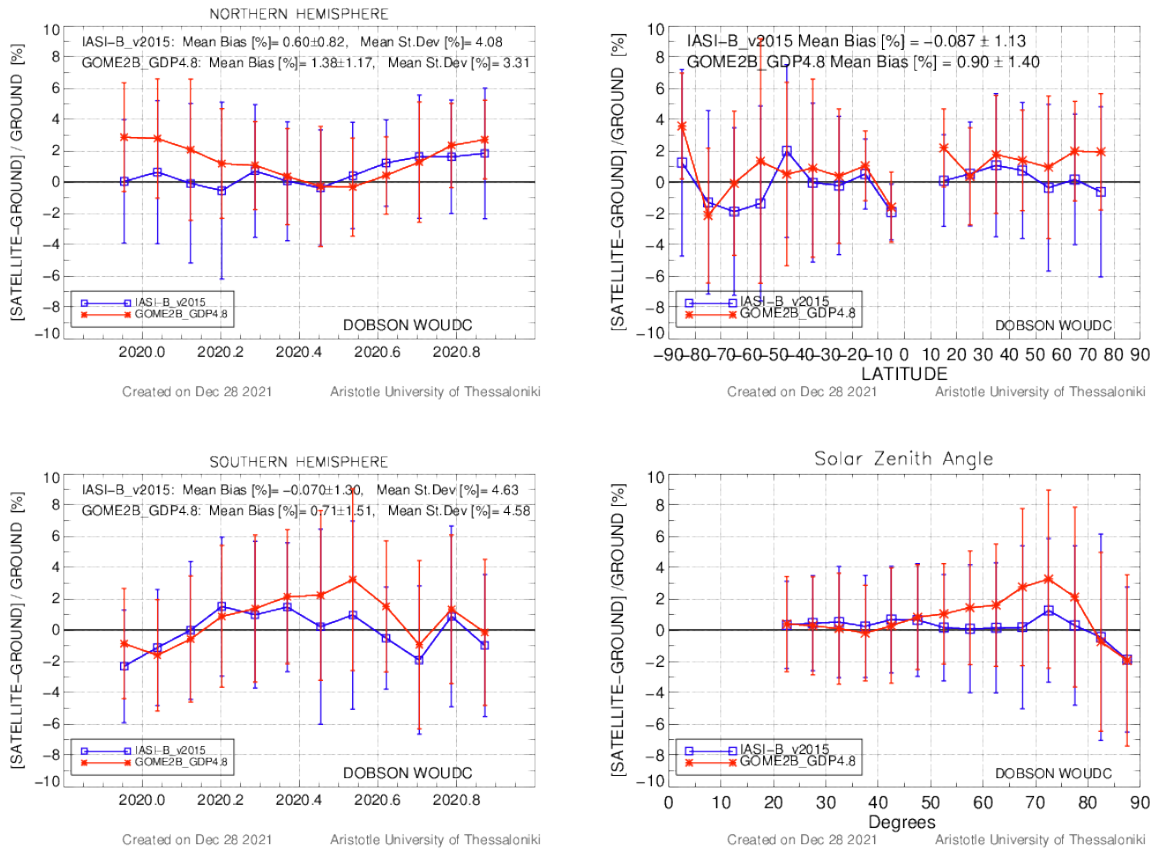

Figure 4.26: As in Figure 4.25 for IASI-B and GOME-2B

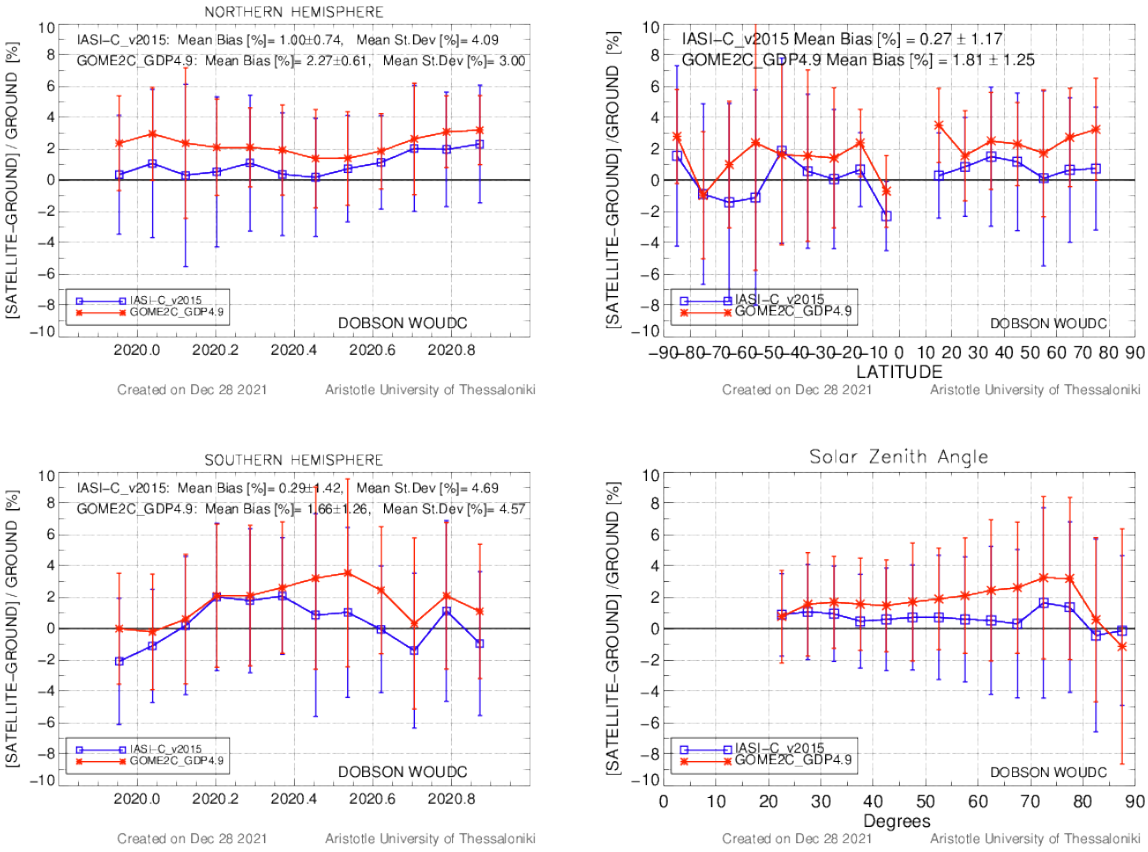

Figure 4.27: As in Figure 4.25 for IASI-C and GOME-2C.

4.5 Conclusions from the of IASI-A, IASI-B and IASI-C total ozone validation

The IASI-A, IASI-B and IASI-C total ozone products, retrieved with the FORLI v20151001 algorithm implemented by EUMETSAT, covering the time period November 2019 – December 2020, were validated against ground-based daily total ozone measurements from Dobson and Brewer instruments, downloaded from WOUDC. The products under validation were also compared to the temporally and spatially co-located operational total ozone products from GOME-2A, GOME-2B (retrieval algorithm GDP4.8) and GOME-2C (retrieval algorithm GDP4.9), to further assess their consistency. Therefore, three types of comparisons were performed:

- the IASI-A, IASI-B and IASI-C TOC data were firstly compared to archived ground-based Dobson and Brewer total ozone measurements (Section 0),

- then the three IASI instruments were indirectly inter-compared, over the same ground-based observational network (Section 0),
- and thirdly, they were indirectly inter-compared to the respective GOME-2A, GOME-2B and GOME-2B operational total ozone products (Section 0).

The co-locations of the IASI sensors were not filtered by the **O3_QFLAG** parameter, as it is suggested by the PUM. The decision not to apply this filter came as a result of an investigation that showed if it was applied the number of co-locations that would be left out of our analysis would be extremely high, about 90%. **It is recommended that this flag is re-evaluated.**

The validation results can be summarized to the following points:

- The **mean relative bias** of the comparisons of the three IASI satellite instruments and the co-located ground-based total ozone observations, as shown in the summary Table 4.6, is always positive and **ranges between 0% and 0.7%.** Note that the Brewer statistics in Table 4.6 are based on the northern hemisphere only, nonetheless they result from the double number of co-locations. The mean standard deviation is 4.4 – 4.6% for all comparisons and **the correlation coefficient is always above 0.94,** showing an excellent agreement between the IASI instruments and the ground-based networks. The seasonal variability of the comparisons could not be studied due to the limited temporal range of the dataset. The latitudinal analysis of the comparisons with respect to Dobson observations, showed **a higher mean bias for the southern hemisphere high latitude station of Amundsen-Scott of 3-4%**, suggesting that the FORLI v20151001 algorithm overestimates total ozone in the Antarctic, which agrees with previous studies. Finally, **the intercomparison of the three IASI sensors showed that they are in excellent spatial-temporal agreement**.
- The IASI co-locations to ground-based observations of total ozone were also used to investigate the dependence of the satellite product on various influence quantities, such as cloud and surface properties. It was found that, even though the datasets were not filtered with the O3_QFLAG parameter which includes the restriction that cloud fraction should be less than 13%, the comparisons have no dependence on any cloud property. On the contrary, it was seen that **very low surface temperatures, like those observed in Antarctica, strongly affect the satellite products resulting to an overestimation of total ozone of ~20-40%**, depending on the temperature.
- The indirect **comparison of IASI instruments against the respective GOME2** sensors showed that they agree very well, **within 0.5 %**, with IASI reporting lower TOCs than GOME2 in all datasets under investigation.

To summarize, the IASI-A, IASI-B and IASI-C total ozone columns processed with the FORLI v20151001 algorithm by EUMETSAT are products of very good quality. The re-evaluation of the O3_QFLAG is necessary so as the product users to be able to follow the PUM instructions, even though it was shown that the validation results were very satisfying without applying any filtering to the available dataset.

Table 4.6: Mean relative differences and mean standard deviation of the comparisons between IASI-A, IASI-B and IASI-C total ozone and ground-based observations.

Satellite product	Ground-based network	Mean rel. Bias (%)	Mean std (%)	R^2	Nobs
IASI-A FORLI_v20151001	Dobson	0.1	4.6	0.95	5707
	Brewer (NH)	0.2	4.6	0.94	12086
IASI-B FORLI_v20151001	Dobson	0.3	4.5	0.95	5724
	Brewer (NH)	0.2	4.6	0.94	12176
IASI-B FORLI_v20151001	Dobson	0.7	4.5	0.95	5646
	Brewer (NH)	0.5	4.4	0.94	12041

Table 4.7: The overall difference in mean relative bias between the IASI and GOME-2 co-locations to the same ground-based measurements.

Satellite product	Ground-based network	Difference in Mean rel. Bias (%)
IASI-A vs GOME-2	Dobson	-0.1
	Brewer (NH)	-0.2
IASI-B vs GOME-2B	Dobson	-0.3
	Brewer (NH)	-0.2
IASI-B vs GOME-2C	Dobson	-0.7
	Brewer (NH)	-0.5

5.General conclusions

The IASI ozone profile and total ozone products have been extensively examined by validating them against different ground truth observations (ozone sondes, lidar, microwave observations for the profile data; Brewer and Dobson observations for examining the integrated profile).

When looking at the integrated ozone profile products, processed with the FORLI v20151001 algorithm by EUMETSAT, and retrieved from the IASI-A/B/C sensors, we can conclude that these products are of very good quality:

- The comparisons of the ozone profile product with ozonesondes, lidar and microwave instruments for all sensors show almost exactly the same results. In the stratosphere the optimal value of 5% is met for the mid-latitudes. In the tropical and high-latitude upper stratosphere the optimal value is slightly exceeded (Table 3.2). In the troposphere, the target value (30 %) (according to Table 2.3) is reached.
- In general, we observe an underestimation in the troposphere and the lower stratosphere. The UTLS zone shows an overestimation.
- When looking at the upper stratosphere, we observe a significant overestimation.
- IASI ozone profile retrievals show a seasonal dependency, especially higher up in the profile and is also latitudinal dependent (more influenced towards the poles).

The main conclusions for the IASI-A/B/C total ozone products, also processed with the FORLI v20151001 algorithm by EUMETSAT, are:

- The mean relative bias of the comparisons to the co-located ground-based total ozone observations (Table 4.6), ranges between 0% and 0.7%. The mean standard deviation is 4.4 – 4.6% for all comparisons and the correlation coefficient is always above 0.94, showing an excellent agreement between the IASI instruments and the ground-based networks. It was also seen that very low surface temperatures, like those observed in Antarctica, strongly affect the satellite products resulting to an overestimation of total ozone of ~20-40%, depending on the temperature. Nevertheless, the products are within the optimal accuracy requirements (Table 1.2).
- The indirect comparison of IASI instruments against the respective GOME2 sensors showed that they agree very well, within 0.5 % (Table 4.7), with IASI reporting lower TOCs than GOME2 in all datasets under investigation.
- The re-evaluation of the O3_QFLAG is necessary so as the product users to be able to follow the PUM instructions, even though it was shown that the validation results were very satisfying using without applying any filtering to the available dataset.

6.References

Antón, M., Loyola, D., López, M., et al.: Comparison of GOME-2/MetOpA total ozone data with Brewer spectroradiometer data over the Iberian Peninsula, Annales Geophysicae, 27, 1377–1386, DOI:10.5194/angeo-27-1377-2009, 2009.

Balis, D., Kroon, M., Koukouli, M. E., et al.: Validation of Ozone Monitoring Instrument total ozone column measurements using Brewer and Dobson spectrophotometer ground-based observations, J. Geophys. Res., 112, D24S46, doi:10.1029/2007JD008796, 2007a

Balis, D., Lambert, J.-C., Van Roozendael, M., Spurr, R., Loyola, D., Livschitz, Y., Valks, P., Amiridis, V., Gerard, P., Granville, J., Zehner, C.: Ten years of GOME/ERS2 total ozone data—The new GOME data processor (GDP) version 4: 2. Ground-based validation and comparisons with TOMS V7/V8, J. Geophys. Res., 112, D07307, doi:10.1029/2005JD006376, 2007b

Eumetsat, IASI Level2: Product Format Specification, EPS.MIS.SPE.980760, 2017

Garane, K., Lerot, C., Coldewey-Egbers, M., Verhoelst, T., Koukouli, M. E., Zyrichidou, I., Balis, D. S., Danckaert, T., Goutail, F., Granville, J., Hubert, D., Keppens, A., Lambert, J.-C., Loyola, D., Pommereau, J.-P., Van Roozendael, M., and Zehner, C.: Quality assessment of the Ozone_cci Climate Research Data Package (release 2017) – Part 1: Ground-based validation of total ozone column data products, Atmos. Meas. Tech., 11, 1385–1402, https://doi.org/10.5194/amt-11-1385-2018, 2018

Garane, K., Koukouli, M.-E., Verhoelst, T., Lerot, C., Heue, K.-P., Fioletov, V., Balis, D., Bais, A., Bazureau, A., Dehn, A., Goutail, F., Granville, J., Griffin, D., Hubert, D., Keppens, A., Lambert, J.-C., Loyola, D., McLinden, C., Pazmino, A., Pommereau, J.-P., Redondas, A., Romahn, F., Valks, P., Van Roozendael, M., Xu, J., Zehner, C., Zerefos, C., and Zimmer, W.: TROPOMI/S5P total ozone column data: global ground-based validation and consistency with other satellite missions, Atmos. Meas. Tech., 12, 5263–5287, https://doi.org/10.5194/amt-12-5263-2019, 2019

Garane, K., M. Koukouli, D. Balis, K.-P. Heue, P. Valks: AC SAF GOME2-C Total Ozone Validation Report, SAF/AC/AUTH/VR/O3, May 2020.

Hao, N., Koukouli, M. E., Inness, A., Valks, P., Loyola, D. G., Zimmer, W., Balis, D. S., Zyrichidou, I., Van Roozendael, M., Lerot, C., and Spurr, R. J. D.: GOME-2 total ozone columns from MetOp-A/MetOp-B and assimilation in the MACC system, Atmos. Meas. Tech., 7, 2937–2951, https://doi.org/10.5194/amt-7-2937-2014, 2014.

Koukouli, M, Zyrichidou, I., Balis, D., Valks, P. and N. Hao, O3M-SAF GOME-2A and GOME-2B Total Ozone Validation Report, SAF/O3M/AUTH/VRR/O3, December 2015.

Koukouli, M. E., Balis, D. S., Loyola, D., Valks, P., Zimmer, W., Hao, N., Lambert, J.-C., Van Roozendael, M., Lerot, C., and Spurr, R. J. D.: Geophysical validation and long-term consistency between GOME-2/MetOp-A total ozone column and measurements from the

sensors GOME/ERS-2, SCIAMACHY/ENVISAT and OMI/Aura, Atmos. Meas. Tech., 5, 2169–2181, https://doi.org/10.5194/amt-5-2169-2012, 2012.

Koukouli, M. E., Zyrichidou, I., Balis, D. S., Valks, P., Hao, N., and Valks, P.: GOME-2/MetopA & GOME-2/MetopB GDP 4.8 total ozone data validation for MetOp-B Operational Readiness Review, Technical Note/Validation Report SAF/O3M/AUTH/VRR/O3, O3M SAF, available at: https://acsaf.org/docs/vr/Validation_Report_NTO_OTO_DR_O3_GDP48_Dec_2015.pdf (last access: 5 January 2022), 2015

Loyola, D., Koukouli, M., Valks, P., Balis, D., Hao, N., Van Roozendael, M., Spurr, R., Zimmer, W., Kiemle, S., Lerot, C., and Lambert, J-C.: The GOME-2 Total Column Ozone Product: Retrieval Algorithm and Ground-Based Validation, J. Geophys. Res., 116, D07302, doi:10.1029/2010JD014675, 2011.

Valks, P., L. Chan, P. Hedelt, S. Slijkhuis, R. Lutz: Algorithm Theoretical Basis Document for GOME-2 Total Column Products of Ozone, NO2, BrO, HCHO, SO2, H2O, OClO and Cloud Properties, GDP 4.8 for GOME-2 on MetOp-A and -B , GDP 4.9 for GOME-2 on MetOp-C (last access 9/1/2022), November 2019

APPENDIX I

Table A. 1: List of Brewer ground-based stations used for the comparisons

STATION ID	NAME	COUNTRY	LONGITUTE (degrees)	LATITUDE (degrees)	Last day of available measurement
12	Sapporo	Japan	141.33	43.06	30-NOV-2020
14	Tateno	Japan	140.13	36.05	30-NOV-2020
21	Edmonton	Canada	-114.10	53.55	30-NOV-2020
24	Resolute	Canada	-94.98	74.72	03-OCT-2020
53	Uccle	Belgium	4.36	50.80	31-OCT-2020
65	Toronto	Canada	-79.47	43.78	30-NOV-2020
76	Goose	Canada	-60.39	53.29	30-NOV-2020
77	Churchill	Canada	-93.82	58.74	30-NOV-2020
89	Ny Alesund	Norway	11.92	78.92	03-NOV-2020
95	Taipei	Taiwan	121.48	25.02	23-NOV-2020
96	Hradec Kralove	Czech Republic	15.84	50.18	30-NOV-2020
99	Hohenpeissenberg	Germany	11.01	47.80	28-NOV-2020
190	Naha	Japan	127.68	26.20	30-NOV-2020
213	El Arenosillo	Spain	-6.73	37.10	30-NOV-2020
261	Thessaloniki	Greece	22.96	40.63	26-NOV-2020
279	Norkoping	Sweden	16.15	58.58	29-NOV-2020
282	Kislovodsk	Russia	42.66	43.73	31-MAR-2020
284	Vindeln	Sweden	19.77	64.23	30-OCT-2020
290	Saturna	Canada	-123.13	48.78	30-NOV-2020
295	Mt Waliguan	China	100.90	36.29	30-NOV-2020
308	Madrid	Spain	-3.72	40.45	30-NOV-2020
315	Eureka	Canada	-86.42	80.05	30-NOV-2020
316	Debilt	Netherlands	5.18	52.10	30-NOV-2020
318	Valentia	Irland	-10.25	51.94	31-OCT-2020
326	Longfenshan	China	127.60	44.73	30-NOV-2020
330	Hanoi	Vietnam	105.80	21.20	30-NOV-2020
331	Poprad-Ganovce	Slovakia	20.32	49.03	30-NOV-2020
346	Murcia	Spain	-1.17	38.00	30-NOV-2020
352	Manchester	United Kingdom	-2.23	53.47	28-NOV-2020
353	Reading	United Kingdom	-0.94	51.44	27-NOV-2020
376	Mrsa Mtrouh	Egypt	27.22	31.33	31-OCT-2020
401	Santa_Cruz	Spain	-16.25	28.47	30-NOV-2020
405	La Coruna	Spain	-8.47	43.33	30-NOV-2020

411	Zaragoza	Spain	-0.91	41.63	30-NOV-2020
435	Paramaribo	Suriname	-55.21	5.81	30-NOV-2020
456	Care	Canada	-79.78	44.23	30-NOV-2020
476	Andoya	Norway	16.01	69.28	09-OCT-2020
479	Aosta	Italy	7.36	45.74	30-NOV-2020

Table A. 2: List of Dobson ground-based stations used for the comparisons.

STATION ID	NAME	COUNTRY	LONGITUTE (degrees)	LATITUDE (degrees)	Last day of available measurement
2	Tamanrasset	Algeria	5.52	22.78	30-NOV-2020
10	New Delhi	India	77.17	28.63	30-NOV-2020
14	Tateno	Japan	140.13	36.05	30-NOV-2020
19	Bismarck	USA	-100.75	46.76	30-NOV-2020
27	Brisbane	Australia	153.08	-27.42	30-NOV-2020
29	Macquarie Island	Australia	158.94	-54.49	30-NOV-2020
31	Mauna Loa	USA	-155.58	19.54	30-NOV-2020
43	Lerwick	UK	-1.18	60.13	25-NOV-2020
57	Halley Bay	Antarctica	-26.18	-75.62	30-SEP-2020
67	Boulder	USA	-105.26	39.99	30-NOV-2020
68	Belsk	Poland	20.79	51.84	30-NOV-2020
82	Lisbon	Portugal	-9.13	38.76	23-NOV-2020
84	Darwin	Australia	130.88	-12.42	30-NOV-2020
96	Hradec Kralove	Czech Republic	15.84	50.17	20-NOV-2020
99	Hohenpeissenberg	Germany	11.01	47.80	27-NOV-2020
101	Syowa	Antarctica	39.58	-69.00	30-NOV-2020
105	Fairbanks	USA	-147.87	64.82	22-OCT-2020
107	Wallops Island	USA	-75.46	37.94	25-NOV-2020
111	Amundsen-Scott	Antarctica	-24.80	-89.99	30-NOV-2020
152	Cairo	Egypt	31.28	30.08	29-NOV-2020
191	Samoa	USA	-170.56	-14.25	29-NOV-2020
199	Barrow	USA	-156.61	71.32	07-OCT-2020
208	Shiangher	China	116.96	39.75	30-NOV-2020
216	Bangkok	Thailand	100.62	13.67	30-NOV-2020
219	Natal	Brazil	-35.20	-6.00	30-SEP-2020
226	Bucharest	Romania	26.13	44.48	27-NOV-2020
245	Aswan	Egypt	32.78	23.96	30-NOV-2020

252	Seoul	Korea	126.95	37.56	30-NOV-2020
253	Melbourne	Australia	144.83	-37.66	30-NOV-2020
256	Lauder	New Zealand	169.68	-45.04	31-JUL-2020
265	Irene	South Africa	28.22	-25.91	30-NOV-2020
268	Arrival Heights	Antarctica	166.66	-77.83	30-NOV-2020
284	Vindeln	Sweden	19.76	64.23	23-OCT-2020
340	Springbok	South Africa	17.90	-29.67	30-NOV-2020
341	Hanford	USA	-119.63	36.32	30-NOV-2020
409	Hurghada	Egypt	33.75	27.42	30-NOV-2020
410	Amberd	Armenia	44.25	40.38	28-NOV-2020

Table A. 3 List of all ozonesonde stations used for the comparisons

Station	Lat	long	nr of profiles	Last day measure-ment
ALAJUELA	9.98	-84.21	35	27-Nov-20
ASCENSION	-7.98	-14.42	25	25-Nov-20
BROADMEADOWS	-37.69	144.95	53	25-Nov-20
DEBILT	52.1	5.18	57	26-Nov-20
FIJI	-18.1	178.4	16	27-Nov-20
HILO	19.717	-155.083	53	25-Nov-20
HOHENPEISSENBERG	47.8	11.02	138	30-Nov-20
LAUDER	-45.045	169.684	52	27-Oct-20
LA_REUNION	-20.99	55.48	23	24-Nov-20
LERWICK	60.14	-1.19	47	28-Oct-20
MACQUARIE ISLAND	-54.5	158.94	53	26-Nov-20
NAIROBI	-1.27	36.8	7	31-Dec-19
NATAL	-5.42	-35.38	14	25-Nov-20
NEUMAYER	-70.39	-8.15	64	29-Nov-20
PARAMARIBO	5.81	-55.21	44	9-Nov-20
PAYERNE	46.817	6.95	130	30-Oct-20
SAMOA	-14.23	-170.56	40	25-Nov-20
SODANKYLA	67.3666	26.6297	27	9-Jul-20
TATENO-TSUKUBA	36.1	140.1	43	26-Nov-20
UCCLE	50.8	4.35	154	30-Nov-20
VALENTIA	51.93	-10.25	31	11-Nov-20

Table A. 4: List of all lidar and MWR stations used for the comparisons

STATION	Latitude	Longitude	No. of profiles	Last measurement used here

Lidar:				
HOHENPEISSENBERG, Germany	47.8	11.02	1329	30-Nov-2020
OBS. HAUTE PROVENCE, France	43.94	5,71	1164	26-Nov-2020
TABLE MOUNTAIN, Ca., USA	34.4	117.7	2472	28-Nov-2020
MAUNA LOA, Hawaii, USA	19.54	155.58	1355	22-Nov-2020
LAUDER, New Zealand	-45.04	169.68	910	30-Nov-2020
Microwave:				
NY-ALESUND, Spitzbergen, Norway	78.93	11.95	31600	26-Jun-2020
BERN, Switzerland	46.95	7.45	34713	30-Nov-2020
MAUNALOA, Hawaii, USA	19.54	155.58	5374	30-Nov-2020

APPENDIX II

Additional total ozone validation plots with respect to Brewer ground-based measurements.

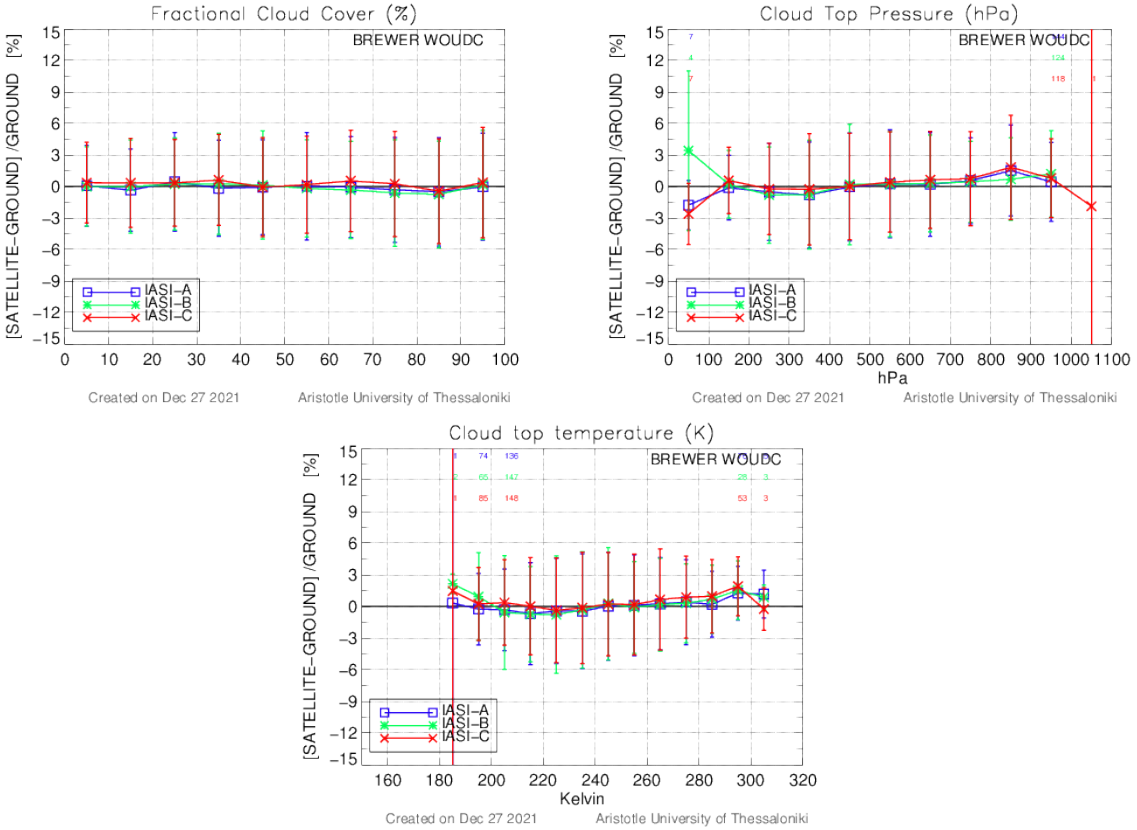

Figure A. 1: As Figure 4.23 for Brewer co-locations

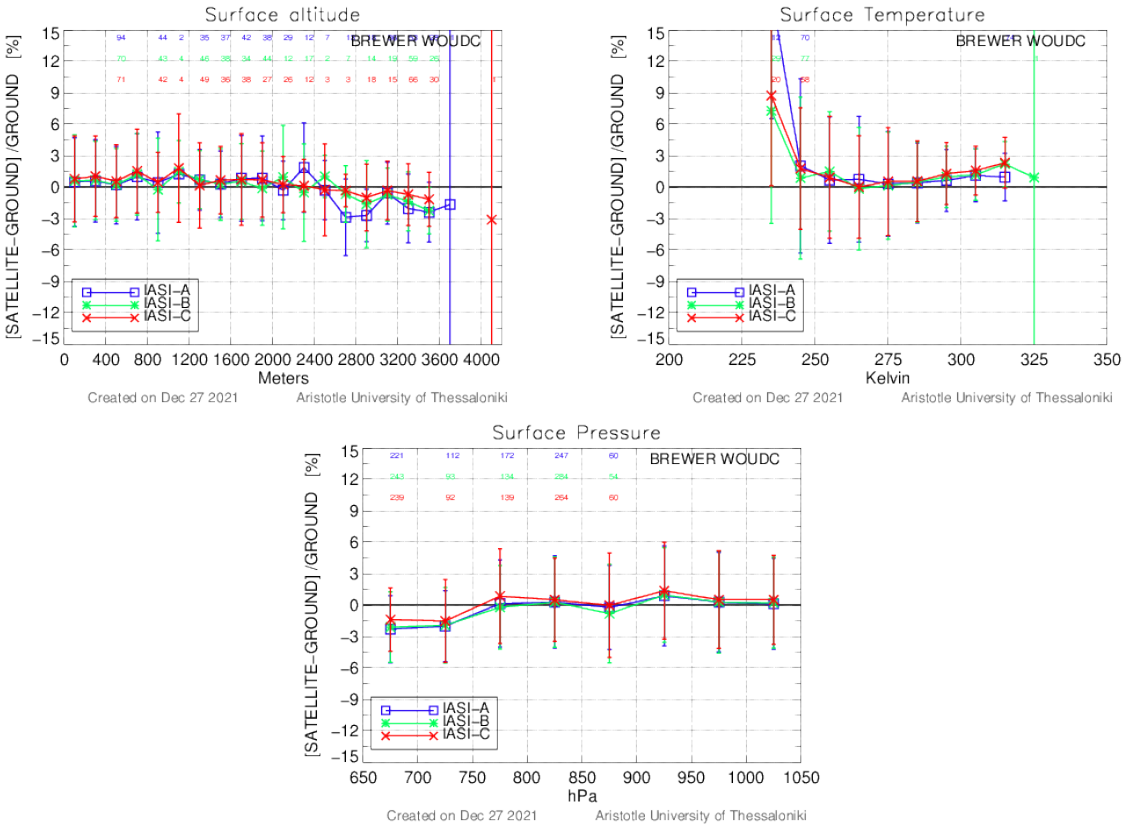

Figure A. 2: As Figure 4.24 for Brewer co-locations

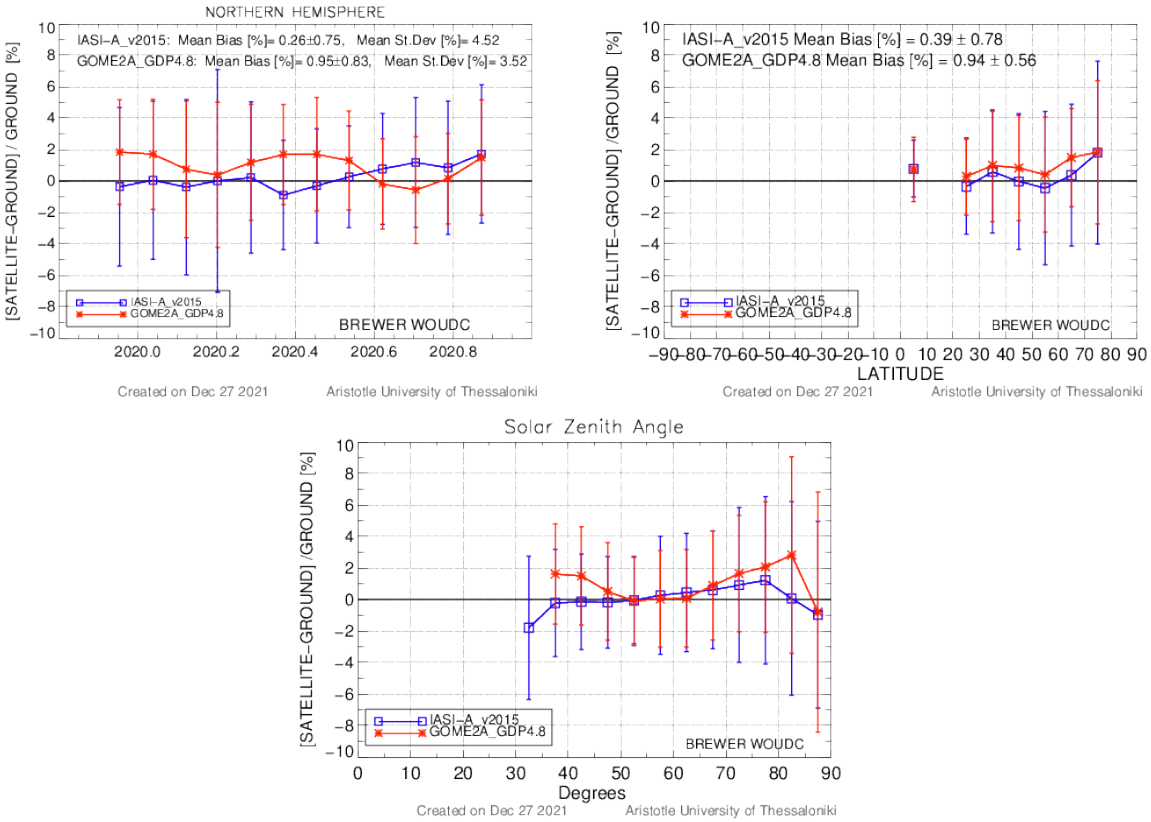

Figure A. 3: As Figure 4.25 for the Brewer and IASI-A co-locations

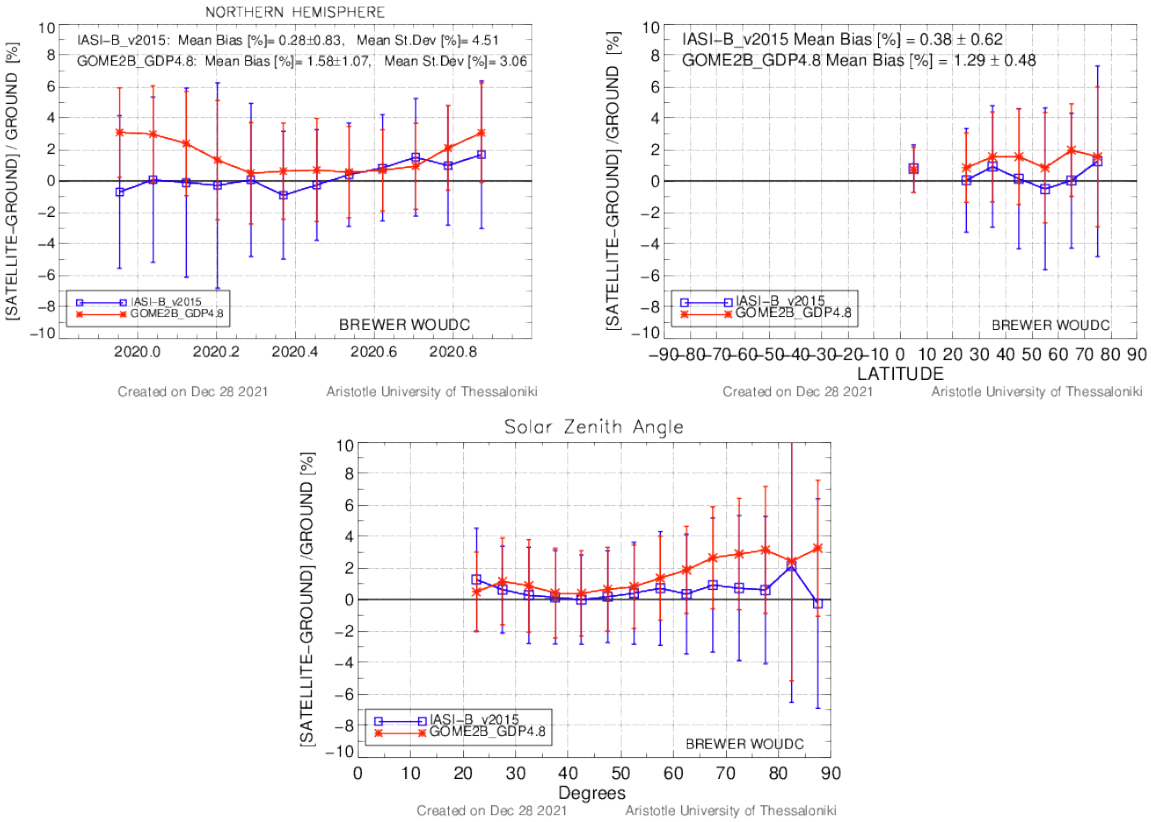

Figure A. 4: As Figure 4.26 for the Brewer and IASI-B co-locations

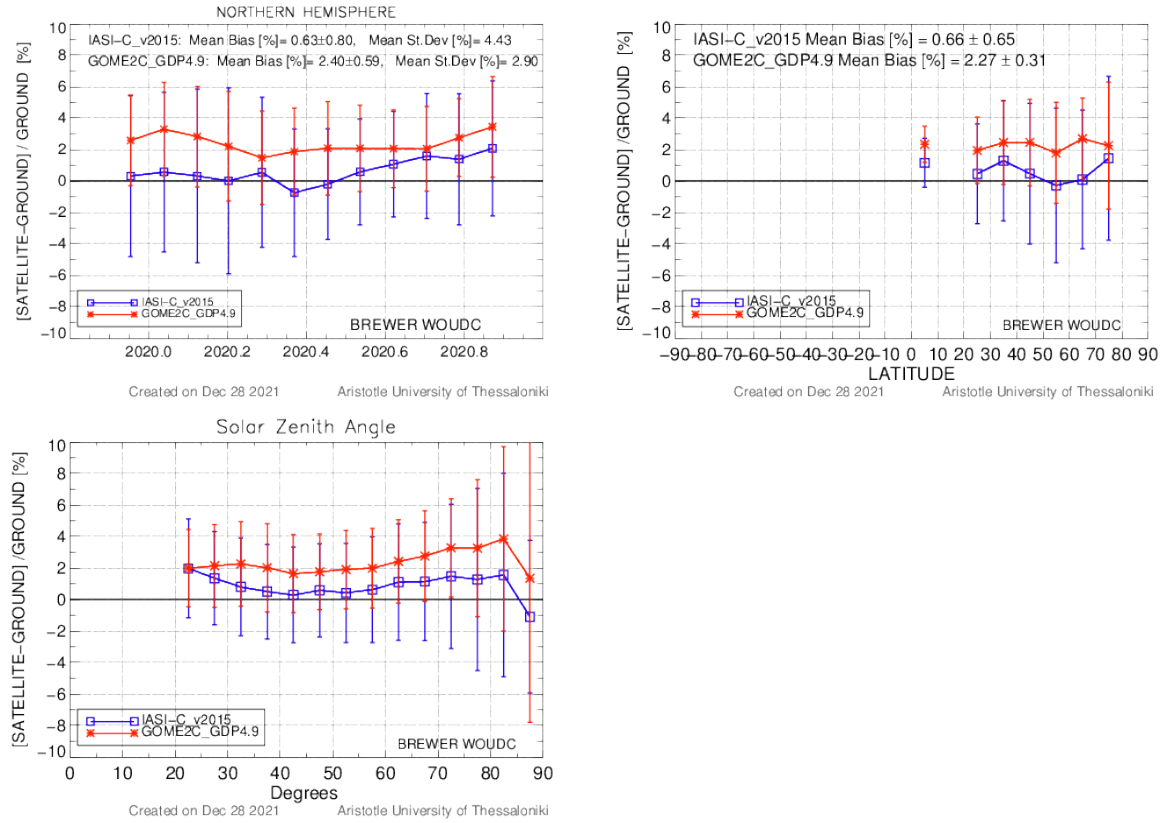

Figure A. 5: As Figure 4.27 for the Brewer and IASI-C co-locations.